Cyanil. Synthesis and Characterization of the Strongest Isolated Electron Acceptor and Its Reduced Forms†

Carlos Vazquez, Joseph C. Calabrese, David A. Dixon,* and Joel S. Miller*

Central Research and Development, Experimental Station E328, Du Pont, Wilmington, Delaware 19880-0328

Received June 23, 1992

The strong acceptor tetracyano-1,4-benzoquinone, cyanil, **Q** [ν(C≡N) at 2210 w and 2241 w cm^{-1}; ν(C=O) at 1697 s cm^{-1} (CH_2Cl_2); ν(C=C) 1616 s cm^{-1} (Raman)], as well as tetracyanohydrobenzoquinone, $\mathbf{QH_2}$ (2241 m and 2263 m cm^{-1}), the radical anion, $[\mathbf{Q}]^{\bullet-}$ [ν(C≡N) ~2216 m cm^{-1} (MeCN)], anion $[\mathbf{QH}]^-$, dianions $[\mathbf{Q}]^{2-}$ (2185 s cm^{-1}), $[\mathbf{H}]^+[\mathbf{Q}]^{2-}$, and the dimer dianion $[\mathbf{Q}]_2^{2-}$ (2217 m and 2226 sh cm^{-1}) have been prepared. $\mathbf{QH_2}$ was prepared from NaCN and *p*-bromanil, and **Q** was prepared from the bromine oxidation of the disilver salt of $\mathbf{QH_2}$, $\mathbf{QAg_2}$. $\mathbf{QAg_2}$ is a versatile synthon for the preparation of **Q**, $[\mathbf{QH}]^-$, $[\mathbf{H}]^+[\mathbf{Q}]^{2-}$, and $[\mathbf{Q}]^{2-}$. The single-crystal X-ray structures of $\mathbf{QH_2}$, $Na^+[H]^+[Q]^{2-}$, $[Me_4N]^+[H]^+[Q]^{2-}$, $[Et_4N]^+[QH]^-$, $[n\text{-}Bu_4N]^+[QH]^-$, $\{[Et_4N]^+\}_2[Q]_2^{2-}$, $\{[(Ph_3P)_2N]^+\}_2[Q]^{2-}$, **Q**, $[Fe(C_5Me_5)_2]^{\bullet+}[H]^+[Q]^{2-}$, and $\{[Fe(C_5Me_5)_2]^{\bullet+}\}_2[Q]_2^{2-}$ have been determined. The average CO (OC–CCN, and NC–CN) distances are 1.204 (1.488, and 1.338), 1.233 (1.463, and 1.378), 1.268 (1.426, and 1.414), and 1.322 (1.413, and 1.372) Å for **Q**, $[\mathbf{Q}]^-$, $[\mathbf{Q}]^{2-}$, and $\mathbf{QH_2}$, respectively. Several salts exhibit very strong intermolecular hydrogen bonding with O···O separations less than 2.5 Å observed for the $[Et_4N]^+[QH]^-$ (2.38 Å), $[Me_4N]^+[H]^+[Q]^{2-}$ (2.43 Å), and $Na^+[H]^+[Q]^{2-}$ (2.48 Å) salts. (The former is the shortest reported for an an organic system with intermolecular hydrogen bonding.) The degree of protonation varies with counterion with examples of $[\mathbf{QH}]^-$ and $[\mathbf{H}]^+[\mathbf{Q}]^{2-}$ being observed and strongly influences the electronic and ν(C≡N) absorptions. The radical anion was structurally characterized as its diamagnetic dimer dianion, $[\mathbf{Q}]_2^{2-}$, with an intradimer separation of 2.88 Å. The EPR of $[\mathbf{Q}]^{\bullet-}$ in dilute CH_2Cl_2/MeCN displays hyperfine interaction with four equivalent nitrogens (a_{CN} = 0.32 G) and two types of ^{13}C (2.58 and 5.25 G). Cyanil is the strongest acceptor that has been isolated in the neutral form and has three quasi-reversible one-electron reductions at 0.90, 0.09, and −1.81 V vs SCE in MeCN. It is unstable in aqueous media. The reduction potential of cyanil is 0.30 V or more greater than those of DDQ, $n\text{-}C_4(CN)_6$, and perfluoro-7,7,8,8-tetracyano-*p*-quinodimethane ($TCNQF_4$). **Q** dehydrogenates 2,3-dichloro-5,6-dicyanohydroquinone (H_2DDQ); thus it is a stronger hydrogen abstraction reagent than conventionally used DDQ. Molecular orbital (ab initio) calculations are in general agreement with the above results, and optimized geometries were used to understand the complex crystal structures.

Introduction

Donor/acceptor (D/A) complexes have been studied for many decades.[1] With their extension to electron-transfer salts[2-4] these complexes led to the 1960 discovery of molecule-based, metal-like conductors[5,6] and the 1980s discoveries of molecule-based superconductors[7] and ferromagnets.[8,9] With the anticipation of finding additional examples of materials exhibiting such properties, improving the physical properties and raising the critical temperatures as well as discovering new phenomena, new donors and acceptors continue to be the subject of intense study.

Many strong acceptors are based upon 1,4-benzoquinones, e.g., the anils. As evidenced by comparison of tetrachloro-1,4-benzoquinone (chloranil) with 2,3-dichloro-5,6-dicyano-1,4-benzoquinone, DDQ, the replacement of the halide with the cyano group leads to a stronger acceptor. The fully cyano-substituted anil, tetracyano-1,4-benzoquinone, cyanil, **Q**, is expected to be a substantially

† Contribution No. 6040.

(1) Mulliken, R. S.; Person, W. B. *Molecular Complexes: A Lecture and Reprint Volume*; Wiley: New York, 1969. Soos, Z. G. *Annu. Rev. Phys. Chem.* **1974**, *25*, 121. Mulliken, R. S. *J. Phys. Chem.* **1952**, *56*, 801.

(2) See, for example: *Extended Linear Chain Compounds*; Miller, J. S., Ed.; Plenum Publisher Corp.: New York, 1982, 1983; Vols. 1-3. Simon, J.; André, J. J. *Molecular Semiconductors*; Springer Verlag: New York, 1985.

(3) For a detailed overview, see the proceedings of the recent series of international conferences: *Syn. Met.* **1988**, *27*; **1989**, *28*, *29* (Aldissi, M., Ed.); *Mol. Cryst. Liq. Cryst.* **1985**, *117-121* (Pecile, C., Zerbi, G., Bozio, R., Girlando, A., Eds.); *J. Phys. (Paris) Collogue* **1983**, *44-C3* (Comes, R., Bernier, P., André, J. J., Rouxel, J., Eds.); *Mol. Cryst. Liq. Cryst.* **1981**, *77*, *79*, *82*, *83*, *85*; **1982** *86* (Epstein, A. J., Conwell, E. M., Eds.); *Chem. Scr.* **1981**, *17* (Carneiro, K., Ed.); *Lecture Notes Phys.* **1979**, *95* and *96* (Bartsic, S., Bjelis, A., Cooper, J. R., Leontic, B. A., Eds.); *Ann. N.Y. Acad. Sci.* **1978**, *313* (Miller, J. S., Epstein, A. J., Eds.).

(4) Epstein, A. J.; Miller, J. S. *Sci. Am.* **1979**, *241* (4), 52. Bechgaard, K.; Jerome, D. *Sci. Am.* **1982**, *247* (2), 52.

(5) Acker, D. S.; Harder, R. J.; Hertler, W. R.; Mahler, W.; Melby, L. R.; Benson, R. E.; Mochel, W. E. *J. Am. Chem. Soc.* **1960**, *82*, 6408. Kepler, R. G.; Bierstedt, P. E.; Merrifield, R. E. *Phys. Rev. Lett.* **1960**, *5*, 503.

(6) Melby, L. R.; Harder, R. J.; Hertler, W. R.; Mahler, W.; Benson, R. E.; Mochel, W. E. *J. Am. Chem. Soc.* **1962**, *84*, 3374. Shchegolev, I. F.; Buravov, L. I.; Zvarykina, A. V.; Lyubovskii, R. B. *JETP Lett.* **1968**, *8*, 218.

(7) Williams, J. M.; Carnerio, K. *Adv. Inorg. Chem. Radiochem.* **1985**, *29*, 249. Chaikin, P. M.; Greene, R. L. *Phys. Today* **1986**, *31* (5), 24. Jerome, D.; Bechgaard, K. *Contemp. Phys.* **1982**, *23*, 583. Williams, J. M. *Prog. Inorg. Chem.* **1985**, *33*, 183.

(8) (a) Chittipeddi, S.; Cromack, K. R.; Miller, J. S.; Epstein, A. J. *Phys. Rev. Lett.* **1987**, *58*, 2695. Miller, J. S.; Calabrese, J. C.; Bigelow, R. W.; Epstein, A. J.; Zhang, R. W.; Reiff, W. M. *J. Chem. Soc., Chem. Commun.* **1986**, 1026. (b) Miller, J. S.; Calabrese, J. C.; Rommelmann, H.; Chittipeddi, S.; Zhang, J. H.; Reiff, W. M.; Epstein, A. J. *J. Am. Chem. Soc.* **1987**, *109*, 769.

(9) (a) Miller, J. S.; Epstein, A. J.; Reiff, W. M. *Chem. Rev.* **1988**, *88*, 201. (b) Miller, J. S.; Epstein, A. J. *NATO Adv. Studies Ser. B* **1988**, *168*, 159. (c) Miller, J. S.; Epstein, A. J.; Reiff, W. M. *Acc. Chem. Res.* **1988**, *21*, 114. (d) Miller, J. S.; Epstein, A. J.; Reiff, W. M. *Science* **1988**, *240*, 40. Miller, J. S.; Epstein, A. J. *New Aspects of Organic Chemistry*; Yoshida, Z., Shiba, T., Ohsiro, Y., Eds.; VCH Publishers: New York, 1989; p 237. Buchachenko, A. L. *Russ. Chem. Rev.* **1990**, *59*, 307; *Usp. Khim.* **1990**, *59*, 529.

0022-3263/93/1958-0065$04.00/0

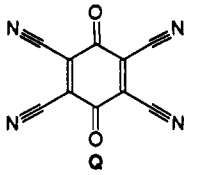

Q

stronger acceptor, but it has not been characterized. Because strong acceptors enable the formation of electron-transfer D/A salts, cyanil might form the desired ···$D^{\bullet+}A^{\bullet-}D^{\bullet+}A^{\bullet-}$··· 1D structure (e.g., with decamethylferrocene) which appears to be a useful structure in the synthesis of a molecular ferromagnet,[9] and thus its preparation was sought. However, a reproducible synthesis and the detailed characterization of the physical and chemical properties of **Q** have not as yet been reported.

Wallenfels and co-workers described the synthesis of **Q** from 2,5-dibromo-3,6-dicyanobenzoquinone to form tetracyanohydroquinone, $\mathbf{QH_2}$, which was oxidized to **Q** with "nitrose gase".[10] Also in 1965 Webster et al. reported the preparation of $\mathbf{QH_2}$ from tetracyanoethylene via the diazonium salt of 1,4-diaminotetracyanobenzene.[11] Later Friedrich et al. reported an "improved synthesis"; a five-step procedure from chloranil, bromanil, or DDQ, with 5, 7, and 3% overall yields of $\mathbf{QH_2}$, respectively.[12] However, we were unable to obtain **Q** from these simpler syntheses. Herein we report a new procedure for the synthesis of **Q** together with a wide range of physical and theoretical studies for **Q**, $[\mathbf{QH}]^-$, $\mathbf{QH_2}$, $[\mathbf{Q}]^{\bullet-}$, and $[\mathbf{Q}]^{2-}$.

Experimental Section

All reactions were performed in a Vacuum Atmospheres Dri-Box under a nitrogen atmosphere unless noted. Elemental analyses were performed by Oneida Research Services, Inc. (Whitesboro, NY). Cyclic voltammetry at 100 mV/s was performed in acetonitrile solution containing 0.1 M $[n\text{-}Bu_4N][ClO_4]$ electrolyte in a conventional H cell with a platinum working electrode and Ag/AgCl reference electrode. All reported potentials are vs SCE. Voltammograms were recorded with a Princeton Applied Research 173/175 potentiostat/programmer. Magnetic susceptibility data were recorded using the Faraday technique from ~2 to 320 K.[13] Infrared spectra were recorded on a Nicolet 7199 Fourier transform spectrometer. Electronic absorption spectra in the range 200–1400 nm were acquired on a Cary 2300 spectrophotometer. Preliminary emission data were taken with a SPEX 222 photon counting spectrophotometer. All spectra were corrected for spectral sensitivity. Mass spectra were obtained on a VG Micromass 7070HS mass spectrometer using 70 eV electrons as the ionization source. EPR spectra were recorded on an IBM/Bruker ER 200 D-SRC spectrometer. Line positions were measured accurately by using field markers generated by an NMR gaussmeter while the microwave frequency was measured by a microwave frequency counter.

Tetracyanohydroquinone, $\mathbf{QH_2}$. After sodium cyanide (23 g; 472 mmol) was dissolved in 2 L of methanol, *p*-bromanil (Lancaster Syntheses, Windham, NH) (25 g; 59 mmol) was added portionwise over 1 h, the temperature was allowed to rise to 34 °C, and the mixture turned red. This solution was heated under reflux for 45 min before it was rapidly cooled to room temperature. HCl gas was then bubbled into the mixture until it reached a pH between 0 and 1 and was brown in color. This mixture was then concentrated to dryness on a rotary evaporator and the subsequent residue was extracted several times with 1 L of diethyl ether. (Additional solvent permits the extraction of additional unwanted side products.) Morpholine was added to the ether extract until no more solid formed. The red morpholine salt was collected, dried, and recrystallized from a minimal amount of methanol to give 12.5 g of the purified product. The complex was dissolved in a minimum amount of water, and HCl(g) was bubbled in until the mixture became yellow and a solid precipitated. This mixture was extracted with diethyl ether, dried over $MgSO_4$, and evaporated to dryness to yield a yellow solid. The solid was then dissolved in 150 mL of water and filtered to remove insoluble material. HCl gas was bubbled through the filtrate until well-formed yellow crystals precipitated. After extracting with diethyl ether, the remaining yellow solid was dissolved in hot acetic acid, and an equivalent amount of pyrene dissolved in dichloromethane was carefully added. The red complex was collected and washed with dichloromethane. On addition of hot dioxane and cooling, a yellow dioxane complex formed. This product was dissolved in water, filtered, acidified with HCl(g), extracted with Et_2O, dried over $MgSO_4$, concentrated, and recrystallized from acetic acid to produce yellow crystals (1.97 g, 16% yield). Anal. Calcd for $C_{10}H_2N_2O_2$ (Found) C, 57.15 (56.95); H, 0.95 (0.95); N, 26.67 (26.53); and O, 15.24 (15.37). Infrared (Nujol); ν(C≡N) absorptions 2241 m and 2263 m cm^{-1}, ν(OH) 3160 br cm^{-1}. Raman: ν(C≡N) absorptions 2231 s, 2237 s, and 2262 m cm^{-1}. Mp: 373 °C dec. ^{13}C NMR [$Cr(acac)_3$ (acac = acetyl acetonate) added to Me_2CO-d_6]: CN 112.294, CCN 111.217, and COH 155.333 ppm. The high-resolution mass spectrum shows *m/e* at 210.019 806 (calcd 210.017 775 4). In solution $\mathbf{QH_2}$ fluoresces yellow-green [λ_{max} at 429 (22 275 cm^{-1}) and 554 nm (2.24 eV, 18 050 cm^{-1}) in a 1:2 intensity ratio].

Mono(*N,N,N*-triethylethanaminium) salt of 3,6-dihydroxy-1,2,4,5-benzenetetracarbonitrile, $[Et_4N]^+[\mathbf{QH}]^-$, was prepared from the addition of tetraethylammonium iodide (Aldrich), 7.0 g (27 mmol, 2.5 equiv), dissolved in 10 mL of water to a $\mathbf{QH_2}$ solution [2.30 g (10.9 mmol) in 50 mL of hot water]. The solution was boiled for 0.5 h, and the water was reduced to ~10 mL by boiling. Orange needle crystals precipitated upon cooling to room temperature (2.61 g; 71%). The product could also be recrystallized from CH_3CN by Et_2O diffusion. Infrared ν(C≡N) (Nujol) at 2222 m and 2236 w cm^{-1}. No IR absorption assignable to the ν(OH) or δ(OH) was observed. Anal. Calcd for $C_{18}H_{21}N_5O_2$ (Found): C, 63.70 (63.59); H, 6.24 (6.24); and N, 20.64 (20.64).

Mono(*N,N,N*-trimethylmethanaminium) salt of 3,6-dihydroxy-1,2,4,5-benzenetetracarbonitrile monohydrate, $[Me_4N]^+[H]^+[\mathbf{Q}]^{2-}\cdot H_2O$,[14a] was prepared by the above method using $[Me_4N]^+Br^-$ (Aldrich). Anal. Calcd for $C_{14}H_{13}N_5O_2$ (Found): C, 55.86 (56.25); H, 5.02 (4.51); and N, 23.24 (23.17). Infrared (Nujol): ν(C≡N) 2219 m and 2224 sh cm^{-1}.

(10) Wallenfels, K.; Bachman, G. *Angew. Chem.* **1961**, *73*, 142. Wallenfels, K.; Bachman, G.; Hofmann, K.; Kern, R. *Tetrahedron* **1965**, *21*, 2239. Wallenfels, K. A. W.; Bachman, G. U.S. Patent 3 114 756, 1963.

(11) Webster, O. W.; Brown, O. W.; Benson, R. E. *J. Org. Chem.* **1965**, *30*, 3250.

(12) Bucsis, L.; Freidrich, K. *Chem. Ber.* **1976**, *109*, 2462.

(13) Miller, J. S.; Dixon, D. A.; Calabrese, J. C.; Vazquez, C.; Krusic, P. J.; Ward, M. D.; Wasserman, E.; Harlow, R. L. *J. Am. Chem. Soc.* **1990**, *112*, 381.

(14) (a) The nomenclature for the $[H]^+[\mathbf{Q}]^{2-}$ salts is based on $\mathbf{QH_2}$. (b) Without a single-crystal X-ray structure determination we cannot distinguish between $[H]^+[\mathbf{Q}]^{2-}$ salts and $[\mathbf{QH}]^-$ salts.

(15) All crystallographic calculations were performed on a DEC/CRAY computer network, using a system of programs developed by J. C. Calabrese. Plots were made with the ORTEP program (C. K. Johnson, 1971). Direct methods phasing was obtained using MULTAN (P. Main, University of York, England 1980).

(16) GRADSCF is an ab initio gradient program system designed and written by A. Komornicki at Polyatomics Research, Mountain View, CA.

(17) (a) Pulay, P. In *Applications of Electronic Structure Theory*; Schaefer, H. F., III, Ed.; Plenum: New York, 1977; Chapter 4. (b) Komornicki, A.; Ishida, K.; Morokuma, K.; Ditchfield, R.; Conrad, M. *Chem. Phys. Lett.* **1977**, *45*, 595.

(18) (a) King, H. F.; Komornicki, A. *J. Chem. Phys.* **1986**, *84*, 5645. (b) King, H. F.; Komornicki, A. In *Geometrical Derivatives of Energy Surfaces and Molecular Properties*; Jørgenson, P., Simons, J., Eds.; NATO ASI series C. Vol. 166; D. Reidel: Dordrecht, 1986; p 207.

(19) (a) Møller, C.; Plesset, M. S. *Phys. Rev.* **1934**, *46*, 618. (b) Pople, J. A.; Binkley, J. S.; Seeger, R. *Int. J. Quant. Chem. Symp.* **1976**, *10*, 1.

(20) Hehre, W. J.; Stewart, R. F.; Pople, J. A. *J. Chem. Phys.* **1969**, *51*, 2657.

(21) Dunning, T. H., Jr.; Hay, P. J. In *Methods of Electronic Structure Theory*; Schaefer, H. F., III, Ed.; Plenum Press: New York, 1977, Chapter 1.

(22) Slow heterogeneous electron transfer kinetics are apparent from the large peak-to-peak separations.

Disilver(1+) Salt of 3,6-Dihydroxy-1,2,4,5-benzenetetracarbonitrile, QAg_2. A silver nitrate solution [1.29 g (7.6 mmol) in 5 mL of water] was quickly added to a QH_2 solution [0.40 g (0.19 mmol) in 25 mL of hot water]. The mixture turned black, the solid that precipitated was collected by vacuum filtration while warm, and the sample was dried in vacuo (0.79 g, 99%). The infrared spectrum show a strong ν(C≡N) absorption at 2230 s cm^{-1}. Anal. Calcd for $C_{10}N_4Ag_2O_2$ (Found): C, 28.34 (28.05, 28.35); N, 13.22 (12.90, 13.27); and O, 7.55 (8.04).

Cyanil, Tetracyano-1,4-benzoquinone, Q. QAg_2 (0.70 g, 1.65 mmol) was suspended in 40 mL of dry dichloromethane under nitrogen. Bromine (1.06 g, 6.6 mmol) dissolved in 1 mL of dichloromethane was added to the suspension which was stirred at room temperature for 0.5 h. The silver bromide precipitate was filtered off under nitrogen and washed with 3 × 30 mL of dry dichloromethane. After excess solvent was removed and the mixture was cooled to room temperature, small yellow needle crystals formed (0.16 g, 47% yield). Additional product could be obtained from the silver bromide-containing precipitate by further extraction with boiling dichloromethane inside a glovebox. Infrared absorptions: ν(C≡N) at 2210 w and 2241 m cm^{-1}; ν(C=O) at 1697 s cm^{-1} (CH_2Cl_2), 2212 w, 2244 w, 1698 s (Nujol and Fluorolube) cm^{-1}. Attempts to obtain a melting point failed as **Q** started to decompose above 140 °C. Raman absorption: ν(C≡N) 2244 s, ν(C=O) 1695 s, and ν(C=C) 1616 s cm^{-1}. Anal. Calcd for $C_{10}N_4O_2$ (Found): C, 57.70 (57.10); H, 0.0 (0.27); N, 26.92 (26.58); and O, 15.37 (15.95). **Q** was not sufficiently soluble in conventional solvents to obtain a ^{13}C NMR.

In an alternative synthesis, QAg_2 (3.10 g, 7.3 mmol) was quickly added to 50 mL of dry 1,2-dichloroethane containing bromine (4.68 g, 60 mmol) and was stirred under nitrogen for 1 h. The slurry containing AgBr was heated under reflux for 10 min to dissolve the product, and the precipitate was removed by filtration under nitrogen. The precipitate was extracted with 4 × 75 mL of hot 1,2-dichloroethane (in a drybox), and after the solvent was reduced by evaporation, a yellow crystalline solid formed which was collected by vacuum filtration. The solvent was removed from the filtrate yielding additional solids, and the solids were combined (65%, 973 mg).

Mono(*N,N,N*-tributyl-1-butanaminium) salt of 3,6-dihydroxy-1,2,4,5-benzenetetracarbonitrile, $[n\text{-}Bu_4N]^+[QH]^-$, was prepared from **Q** (50 mg; 0.24 mmol) dissolved in 2 mL of acetonitrile. To this solution was added a solution of tetrabutylammonium iodide (Aldrich) (89 mg; 0.24 mmol) in 2 mL of acetonitrile, and the resulting mixture turned green. Into this solution was diffused diethyl ether, and brown needle crystals precipitated. These were collected by vacuum filtration (64 mg; 59% yield). Anal. Calcd for $C_{26}H_{37}N_5O_2$ (Found): C, 69.15 (68.36), H, 8.26 (8.17); N, 15.15 (15.19); and O, 7.09 (7.20). IR (Nujol): ν(C≡N) 2207 m, 2220 m, and 2231 m cm^{-1}; ν(C=O) 1581 cm^{-1}. [No IR absorption assignable to the ν(OH) or δ(OH) was observed.] Raman: ν(C≡N) 2202 s, 2216 s, and 2229 s cm^{-1}.

Monosodium(1+) salt of 3,6-dihydroxy-1,2,4,5-benzenetetracarbonitrile, $Na^+[H]^+[Q]^{2-}$,[14a] was prepared from **Q** (355 mg; 0.169 mmol) dissolved in 10 mL of hot water. To this solution was added 430 mg (5.068 mmol, 3 equiv) of sodium nitrate dissolved in 2 mL of water, and the mixture turned deep-red. After the volume was reduced to 5 mL, the solution was allowed to cool to room temperature and the red-orange crystals which formed were collected and dried under vacuum (0.35 g, 90%). Anal. Calcd for $C_{10}HN_4NaO_2$ (Found): C, 51.74 (51.29); H, 0.43 (0.29); and N, 24.14 (24.03). IR (Nujol): ν(C≡N) 2240 s cm^{-1}. [No IR absorption assignable to the ν(OH) or δ(OH) was observed.] Raman: ν(C≡N) 2237 s and 2247 m cm^{-1}.

Mono(*N,N,N*-triethylethanaminium) salt of 4-hydroxy-2,3,5,6-tetracyanophenoxy, $\{[Et_4N]^+\}_2[Q]_2^{2-}$,[14] was prepared as described above with $[Et_4N]^+I^-$. Long blue needle crystals were collected (36 mg, 60%). Anal. Calcd for $C_{18}H_{20}N_5O_2$ (Found): C, 63.89 (63.88); H, 5.96 (5.71); N, 20.70 (20.61); O, 9.46 (9.69). IR (Nujol): ν(C≡N) 2218 m and 2224 sh cm^{-1}; (MeCN) ν(C≡N) 2216 m cm^{-1}.

Mono(ferrocenium) Salt of 4-Hydroxy-2,3,5,6-tetracyanophenoxy, $[Fe(C_5H_5)_2]^{\bullet+}[Q]^-$,[14] A solution of 39 mg (0.188 mmol) of **Q** dissolved in 5 mL of dry acetonitrile was added to a ferrocene solution (35 mg; 0.188 mmol dissolved in 5 mL dry acetonitrile). The precipitate which formed from the green solution was collected, and after drying 53 mg (72%) of bright-blue needle crystals were isolated. Anal. Calcd for $C_{20}H_{10}FeN_4O_2$ (Found): C, 60.94 (60.75); H, 2.56 (2.50); N, 14.21 (13.88); and O, 15.37 (15.95). Infrared (Nujol): ν(C≡N) 2219 m cm^{-1}.

Mono(decamethylferrocenium) salt of 3,6-dihydroxy-1,2,4,5-benzenetetracarbonitrile, $[Fe(C_5Me_5)_2]^{\bullet+}[H]^+[Q]^{2-}$,[14a] was prepared by the above method in 89% yield and was recrystallized from acetonitrile. Alternatively, $[Fe(C_5Me_5)_2]^{\bullet+}[H]^+[Q]^{2-}$ was prepared in 60% yield from Ag_2Q and 2 equiv of $Fe(C_5Me_5)_2$. Anal. Calcd for $C_{30}H_{31}FeN_4O_2$ (Found): C, 67.29 (67.33); H, 5.84 (5.95); N, 10.46 (10.47); and O, 5.98 (6.20). Infrared (Nujol): ν(C≡N) 2216 m and 2230 w cm^{-1}.

Mono(octamethylferrocenium) salt of 4-hydroxy-2,3,5,6-tetracyanophenoxy, $[Fe(C_5HMe_4)_2]^+[Q]^-$,[14] was prepared by the method used for $[Fe(C_5H_5)_2]^{\bullet+}[Q]^-$ in 60% yield. Anal. Calcd for $C_{28}H_{27}FeN_4O_2$ (Found): C, 66.28 (66.45); H, 5.36 (5.35); and N, 11.04 (11.04). Infrared (Nujol): ν(C≡N) 2216 and 2230 cm^{-1}.

Decamethylferrocenium salt of 4-hydroxy-2,3,5,6-tetracyanophenoxy, $\{[Fe(C_5Me_5)_2]^{\bullet+}\}_2[Q]_2^{2-}$, was prepared from $[Fe(C_5Me_5)_2]^{\bullet+}[BF_4]^-$ [8b] (122 mg; 0.30 mmol) and $[Et_4N]_2[Q]_2$ (100 mg; 0.30 mmol) each dissolved in 3 mL of MeCN; the two solution were rapidly mixed. After the volume was reduced by boiling, the product was collected by vacuum filtration (127 mg; 79%). Infrared (Nujol): ν(C≡N) 2216 m and 2230 sh cm^{-1}.

Mono(tetrathiafulvalenium) salt of 4-hydroxy-2,3,5,6-tetracyanophenoxy, $[TTF]^+[Q]^-$,[14] was prepared from tetrathiofulvalene, TTF (Strem), by the method used for $[Fe(C_5H_5)_2]^{\bullet+}[Q]^-$, giving a 62% yield of copper-like crystals after drying. Anal. Calcd for $C_{16}H_4N_4O_2S_4$ (Found): C, 46.59 (46.34); H, 0.98 (0.89); and N, 13.58 (13.31). Infrared (Nujol): ν(C≡N) 2217 cm^{-1}.

Mono(decamethylchromocenium) salt of 3,6-dihydroxy-1,2,4,5-benzenetetracarbonitrile, $[Cr(C_5Me_5)_2]^+[H]^+[Q]^{2-}$,[14] was prepared by the method used for $[Fe(C_5Me_5)_2]^{\bullet+}[H]^+[Q]^{2-}$ in a 75% yield using THF. After recrystallization from acetonitrile, brown needle crystals suitable of X-ray quality were obtained. Infrared (Nujol): ν(C≡N) 2216 m and 2230 w cm^{-1}. Anal. Calcd for $C_{30}H_{31}CrN_4O_2$ (Found): C, 67.78 (67.08); H, 5.88 (5.37); and N, 10.54 (11.11). Unit cell parameters: a = 19.026 (2) Å, b = 9.843 (2) Å, c = 14.699 (2) Å, β = 96.31 (1)°, V = 2738.4 Å^3, Z = 4, space group is $C2/c$; thus, it is isomorphous to the iron analog.

Mono(decamethylruthocenium) salt of 3,6-dihydroxy-1,2,4,5-benzenetetracarbonitrile, $[Ru(C_5Me_5)_2]^{\bullet+}[H]^+[Q]^{2-}$,[14] was prepared by the method used for $[Fe(C_5Me_5)_2]^{\bullet+}[H]^+[Q]^{2-}$ in 75% yield using MeCN. After recrystallization from acetonitrile, brown needle crystals suitable for X-ray quality were obtained. Infrared (Njuol): ν(C≡N) 2215 s and 2229 m cm^{-1}. Anal. Calcd for $C_{30}H_{31}RuN_4O_2$ (Found): C, 62.05 (62.10); H, 5.38 (4.95); and N, 9.65 (9.66). Unit cell parameters: a = 18.884 (7) Å, b = 9.910 (1) Å, c = 14.673 (5) Å, β = 102.40 (2)°, V = 2681.9 Å^3, Z = 4, space group $C2/c$ at −70 °C. Thus, it is isomorphous to the iron analog. $[Ru(C_5Me_5)_2]^{\bullet+}$, however, is unstable in solution and disproportionates into $Ru^{II}(C_5Me_5)_2$ and $[Ru^{IV}(C_5Me_5)_2]^{2+}$. The latter subsequently deprotonates into $[Ru^{IV}(C_5Me_5)(C_5Me_4CH_2)]^+$, 1.[23] The structure of the anion was determined by X-ray crystallographic methods; however, the cation was disordered and details of the structure are not presented. The disordered cation in the structure of this salt is consistent with the presence of 1 with the methylene moiety disordered over 10 positions and the presence of S = $^1/_2[Ru(C_5Me_5)_2]^{\bullet+}$. From magnetic susceptibility measurements the latter is present to the extent of 7.2%.

Mono(decamethylcobaltocenium) salt of 3,6-dihydroxy-1,2,4,5-benzenetetracarbonitrile, $[Co(C_5Me_5)_2]^+[H]^+[Q]^{2-}$,[14a] was prepared by the method used for $[Fe(C_5Me_5)_2]^{\bullet+}[H]^+[Q]^{2-}$ in 72% yield using THF. After recrystallization from acetonitrile, brown needle crystals suitable for X-ray quality were obtained. Infrared (Nujol): ν(C≡N) 2216 m and 2230 w cm^{-1}. Anal. Calcd for $C_{30}H_{31}CoN_4O_2$ (Found): C, 67.91 (67.13); H, 5.80 (5.20); and N, 10.40 (9.52). Unit cell parameters: a = 18.374 (2) Å, b = 10.043 (2) Å, c = 14.731 (2) Å, β = 96.60 (1)°, V = 2700.3 Å^3, Z

(23) Walker, D.; Hiebert, J. D. *Chem. Rev.* **1966**, *66*, 153. Hydrogen exchange between a quinone and it hydroquinone is unlikely (see: Bothnerby, A. A. *J. Am. Chem. Soc.* **1951**, *73*, 4228.

= 4, space group is $C2/c$; thus, it is isomorphous to the iron analog. Sometimes the blue complex $\{[Co(C_5Me_5)_2]^+\}_2[Q]_2^{2-}$ was isolated; infrared (Nujol): ν(C≡N) 2220 m and 2225 m cm^{-1}.

Mono(hexaazaoctadecahydrocoronenium)(1+) salt of 3,6-dihydroxy-1,2,4,5-benzenetetracarbonitrile, [HOC]$^+$[Q]$^-$, was prepared from hexaazaoctadecahydrocoronene, HOC,[13] and **Q** by the method used for $[Fe(C_5H_5)_2]^{\cdot+}[Q]^-$ in a 73% yield. Anal. Calcd for $C_{28}H_{24}N_{10}O_2$ (Found): C, 63.14 (63.02); H, 4.54 (4.72); and N, 26.31 (26.26). Infrared (Nujol): ν(C≡N) 2217 cm^{-1}.

Bis(decamethylcobaltocenium) salt of 3,6-dihydroxy-1,2,4,5-benzenetetracarbonitrile, $\{[Co(C_5Me_5)_2]^+\}_2[Q]^{2-}$, was prepared by the method used for $[Fe(C_5H_5)_2]^{\cdot+}[Q]^-$ except that $Co(C_5Me_5)_2$ was used in a 2:1 mole ratio (65% yield). Anal. Calcd for $C_{50}H_{60}Co_2N_4O_2$ (Found): C, 69.27 (68.96); H, 6.98 (6.79); N, 6.46 (6.85); and O, 3.69 (4.04). Infrared (Nujol): ν(C≡N) 2181 s and 2194 m cm^{-1}.

Bis(*N,N,N*-tributyl-1-butanaminium) salt of 3,6-dihydroxy-1,2,4,5-benzenetetracarbonitrile, $\{[n\text{-}NBu_4]^+\}_2[Q]^{2-}$, was prepared by the reaction of Ag_2Q [0.220 g (0.52 mmol)] dissolved in 25 mL of MeCN with 0.363 g (1.04 mmol) of tetrabutylammonium iodide in 5 mL of dry acetonitrile. An intense blue color and a fine white precipitate appeared immediately. After the mixture was stirred for 10 min, the precipitate was removed via vacuum filtration. After some of the solvent was removed from the filtrate via boiling, a few milliliters of dry diethyl ether was added and the solution was placed into a refrigerator at −25 °C overnight. Small blue needle crystals unsuitable for X-ray studies formed and were collected by vacuum filtration (0.26 g, 72%). Anal. Calcd for $C_{42}H_{72}N_6O_2$ (Found): C, 72.78 (72.66); H, 10.47 (10.22); and N, 12.13 (12.15). Infrared (Nujol): ν(C≡N) 2187 s cm^{-1}.

Bis(*N,N,N*-triethylethanaminium) salt of 3,6-dihydroxy-1,2,4,5-benzenetetracarbonitrile, $\{[NEt_4]^+\}_2[Q]^{2-}$, was prepared by the above method using tetraethylammonium iodide (71%). Anal. Calcd for $C_{26}H_{41}N_6O_2$ (Found): C, 66.49 (67.00); H, 8.80 (8.60); and N, 17.89 (18.16). Infrared (Nujol): ν(C≡N) 2189 s cm^{-1}. Raman: ν(C≡N) 2226 vw and 2195 s cm^{-1}.

Bis[bis(triphenylphosphine)iminium(V)] salt of 3,6-dihydroxy-1,2,4,5-benzenetetracarbonitrile, $\{[(PPh_3)_2N]^+\}_2[Q]^{2-}$, was prepared by the method used for $\{[n\text{-}NBu_4]^+\}_2[Q]^{2-}$ using bis(triphenylphosphine)iminium(V) chloride (Aldrich) (59%). Anal. Calcd for $C_{82}H_{60}N_6O_2P_4$ (Found): C, 76.63 (76.68); H, 4.71 (4.82); and N, 6.54 (6.45). Infrared (Nujol): ν(C≡N) 2184 s and 2195 w cm^{-1}.

Reaction of Q with 9,10-Dihydroanthracene. A solution of 9,10-dihydroanthracene (35 mg; 0.192 mmol) dissolved in 1 mL of dry acetonitrile was allowed to react with **Q** (40 mg; 0.192 mmol) also dissolved in 1 mL of dry acetonitrile. After the volume was reduced to half and the mixture was cooled to −20 °C, crystals precipitated and were collected. The infrared spectra of the precipitate was identical to that obtained from a mixture of authentic anthracene and H_2Q (ν(C≡N) = 2239 and 2263 cm^{-1}), verifying that **Q** dehydrogenates 9,10-dihydroanthracene.

Reaction of Q with H_2DDQ. The above dehydrogenation was repeated with 2,3-dichloro-5,6-dicyanohydroquinone, H_2DDQ. The IR spectrum of the precipitate was that expected for H_2Q (ν(C≡N) = 2241 and 2264 cm^{-1}), verifying the **Q** dehydrogenates H_2DDQ.

X-ray Structure Determinations. X-ray Data Collection. Crystals of $Na^+[H]^+[Q]^{2-}$, $[Me_4N]^+[H]^+[Q]^{2-}$, $[Et_4N]^+[QH]^-$, $[n\text{-}Bu_4N]^+[QH]^-$, $[Fe(C_5Me_5)_2]^{\cdot+}[H]^+[Q]^{2-}$, $\{[Et_4N]^+\}_2[Q]_2^{2-}$, $\{[Fe(C_5Me_5)_2]^{\cdot+}\}_2[Q]_2^{2-}$, and $\{[(Ph_3P)_2N]^+\}_2[Q]^{2-}$ were grown by diethyl ether diffusion into acetonitrile solutions. QH_2 and **Q** crystals were obtained from dioxane and dichloromethane solution, respectively. Cell constants and an orientation matrix for the data collection were obtained from the diffractometer routines[15] from approximately 25 reflections on a CAD diffractometer with Mo Kα radiation at −70 °C. Systematic absences and subsequent least-squares refinement determined the space groups. During data collection the intensities of several representative reflections were measured as a check on crystal stability. Where there was a loss of intensity during data collection, an isotropic decay correction (<3%), was applied. Equivalent reflections were merged and only those for which $F_o^2 > 3\sigma F_o^2$ were included in the refinement where σF_o^2 is the standard deviation based on counting statistics. Data were also corrected for Lorentz and polarization factors. No absorption correction was made. Crystallographic details are summarized in Table I.

Structure Solution and Refinements. The structures of QH_2, $Na^+[H]^+[Q]^{2-}$, $[Me_4N]^+[H]^+[Q]^{2-}$, $[Et_4N]^+[QH]^-$, $[n\text{-}Bu_4N]^+[QH]^-$, $\{[Et_4N]^+\}_2[Q]_2^{2-}$, $\{[(Ph_3P)_2N]^+\}_2[Q]^{2-}$, and **Q**, were solved by direct methods (MULTAN) while $[Fe(C_5Me_5)_2]^{\cdot+}[H]^+[Q]^{2-}$ and $[Fe(C_5Me_5)_2]^{\cdot+}[Q]^-$ were solved by automated Patterson analysis.[15] The hydrogen atoms were placed at calculated positions [r(C–H) = 0.95 Å]. All structures were refined by full-matrix least-squares of $\sum w[|F_o| - |F_c|]^{1/2}$ with the neutral atom scattering factors taken from the literature.[15] Tables of atomic coordinates, thermal parameters, bond angles, and nonbonding distances are found as supplementary materials.

Molecular Orbital Computations. Ab initio molecular orbital calculations were done with the GRADSCF[16] program on a CRAY X-MP and Y-MP computer systems. Calculations on the closed shell singlet molecules were done with the restricted Hartree–Fock (RHF) formalism, whereas calculations on doublets were done with the restricted open-shell Hartree–Fock (ROHF) formalism. The geometries were gradient optimized.[17] Force fields were calculated analytically.[18] Second-order Møller–Plesset perturbation theory (MP-2) correlation energy calculations were also done on the singlets.[19] The initial calculations were done with the STO-3G basis set.[20] Subsequent calculations were done with a double-ζ basis set augmented by d polarization functions on the six ring carbons and the oxygen atoms.[21]

Results and Discussion

Chemistry. A convenient route to **Q** has been elusive. As outline in Scheme I it can now be easily be prepared from commercially available bromanil (or DDQ) and methanolic NaCN. The first reaction leads to the formation of QH_2 which can be isolated as the charge-transfer complex with dioxane. QH_2 can be subsequently converted to the the disilver salt, QAg_2. This insoluble silver salt is a versatile reagent for the preparation of **Q**, $[QH]^-$, and $[Q]^{2-}$. Oxidation of QAg_2 with bromine directly leads to **Q**.

Cyanil is a yellow crystalline material with three electrochemically quasi-reversible one-electron reductions at potentials of 0.90, 0.09, and −1.81[22] V (vs SCE) in MeCN and 0.90, 0.06, and −1.67[22] V in CH_2Cl_2, respectively. (The cyclic voltammogram is supplied as supplementary material.) Cyanil's reduction potential is more than 0.30 V greater than the strongest previously reported acceptors [i.e., DDQ, $C_4(CN)_6$, and $TCNQF_4$] as shown in Table II. In fact, it is the strongest known acceptor that has been isolated in the neutral form. The acceptors $TCNQ(CN)_4$ and hexacyanotrimethylenecyclopropane, $C_3[C(CN)_2]_3$, have larger reduction potentials (Table II); however, these neutral acceptors have not as yet been isolated. As a consequence, complete electron transfer occurs to **Q** upon reaction with many donors. The protonated dianion, $[QH]^-$, undergoes a quasi-reversible one-electron reduction to $[QH]^{\cdot2-}$ at 1.72 V (vs SCE) as well as a quasi-reversible one-electron oxidation to $[QH]^{\cdot}$ at 0.91 V. Attempts to determine the protic two-electron reduction: $Q + 2H^+ + 2e^- = QH_2$ were thwarted by decomposition in water. It is possible that nucleophilic attack by OH^- leads to substitution of OH for one or more of the CN groups. The radical $[Q]^{\cdot-}$ is evident in solution; however, in the solid it dimerized as $[Q]_2^{2-}$ as characterized for the $[Fe(C_5Me_5)_2]^{\cdot+}$ and $[Et_4N]^+$ salts.

Several intermediates, e.g., QH_2, $[QH]^-$, and $[Q]^{2-}$, were also isolated and characterized. In order to study the acceptor properties of **Q**, several charge-transfer complexes and electron-transfer salts were prepared and characterized. **Q** can also abstract hydrogen from 9,10-dihydroan-

Table I. Summary of Crystallographic Data for Cyanil and Related Compounds

	QH_2-dioxane	$\{[Et_4N]^+\}_2$-$[Q]_2^{2-}$	$Na^+[H]^+$-$[QH]^-$	$[n\text{-}Bu_4N]^+$-$[QH]^-$	$\{[(Ph_3P)_2N]^+\}_2$-$[Q]^{2-}$ [c]	$[Et_4N]^+[QH]^-$	$[Me_4N]^+[H]^+[Q]^{2-}$	cyanil, Q	$[Fe(C_5Me_5)_2]^+$-$[H]^+[Q]^{2-}$	$[Fe(C_5Me_5)_2]_2^+$-$[Q]_2^{2-}$
formula	$C_{14}H_{10}N_4O_4$	$C_{18}H_{20}N_5O_2$	$C_{10}HN_4NaO_2$	$C_{52}H_{73}N_{10}O_4$	$C_{82}H_{60}N_6O_2P_4$	$C_{18}H_{21}N_5O_2$	$C_{14}H_{14}N_5O_2$	$C_{10}N_4O_4$	$C_{30}H_{31}FeN_4O_2$	$C_{30}H_{30}FeN_4O_2$
formula weight	298.26	338.39	232.14	902.2	1285.3	339.40	284.3	208.14	535.45	534.45
color	orange	dark blue	orange	deep red	blue	red	red	yellow	brown	black
crystal dimensions, mm	0.12 × 0.07 × 0.30	0.34 × 0.05 × 0.40	0.30 × 0.02 × 0.46	0.50 × 0.39 × 0.50	0.30 × 0.17 × 0.50	0.37 × 0.26 × 0.52	0.22 × 0.17 × 0.40	0.18 × 0.09 × 0.50	0.25 × 0.03 × 0.43	0.40 × 0.40 × 0.56
space group	$P2_1/c$ (no. 14)	$P2_1/n$ (no. 14)	$P\bar{1}$ (no. 2)	$C2/c$ (no. 15)	$P2_1/c$ (no. 14)	$P2_1/c$ (no. 14)	$P2_1/n$ (no. 14)	$P\bar{1}$ (no. 2)	$C2/c$ (no. 15)	$P2_1/n$ (no. 14)
a, Å	10.850 (50)	6.939 (2)	5.756 (1)	20.113 (4)	9.405 (3)	11.510 (6)	9.076 (4)	9.088 (2)	18.494 (4)	7.401 (5)
b, Å	5.577 (8)	11.760 (2)	6.460 (1)	14.494 (4)	15.504 (3)	24.656 (3)	16.949 (5)	10.325 (3)	9.935 (2)	25.000 (3)
c, Å	11.920 (60)	21.649 (6)	6.957 (3)	14.694 (4)	22.765 (3)	13.318 (6)	9.565 (4)	10.409 (4)	14.671 (4)	14.079 (8)
α, deg	90.00	90.00	85.35 (3)	90.00	90.00	90.00	90.00	95.23 (3)	90.00	90.00
β, deg	109.80 (20)	92.61 (1)	89.00 (3)	90.42 (1)	98.96 (1)	108.76 (2)	91.99 (5)	93.96 (2)	96.46 (1)	94.77 (3)
γ, deg	90.00	90.00	63.92 (1)	90.00	90.00	90.00	90.00	100.68 (2)	90.00	90.00
V, Å^3	678.6	1764.8	231.5	5161.2	3279.0	3581.8	1470.5	952.1	2678.5	2595.9
Z	2	4	1	4	2	8	4	4	4	4
density, g/cm^3	1.459	1.273	1.665	1.161	1.302	1.259	1.284	1.452	1.328	1.367
μ, cm^{-1}	1.03	0.81	1.53	0.70	1.65	0.80	0.85	1.01	5.93	6.12
scan type	ω	ω	ω	ω	ω	ω	ω	ω	ω	ω
scan rate, deg/min (ω)	2.00–2.50	1.50–3.40	1.70–4.00 (ω)	1.70–4.00	1.70–5.00	1.5–5.0	1.5–2.5	1.5–2.5	1.5–2.5	2.5–5.00
scan width, deg ω	1.50–1.80	1.1–1.90	1.30–1.50	1.2–1.80	1.2–1.50	1.20–1.90	1.1–1.80	1.2–1.6	1.2–1.6	1.8–2.4
peak width at half-height, ω, deg	0.26	0.13	0.21	0.14	0.19	0.18	0.14		0.25	0.44
2θ range, deg	3.7–55.0	1.9–52.0	5.9–55.0	2.8–55.0	1.8–48.0	1.7–55.0	3.0–45.8	3.9–52.0	2.8–55	1.6–55
reflections measured (total/unique)	1824/367	3754/1363	1154/810	6340/2601	5496/2035	8725/3160	3592/1717	3962/2097	3370/1292	6335/3733
solution method	direct methods	direct methods	direct methods	direct methods	direct methods	direct methods	direct methods	direct methods	Patterson method	Patterson method
hydrogen atoms	not included	not included	not included	not included	not included	included for ordered cation	not included	none	not included	not included
refinement	[a]	[a]	[a]	[a]	[a]	[a]	diagonal least-squares	[a]	[a]	[a]
minimization function	$\Sigma w(\|F_o\| - \|F_c\|)^2$	$\Sigma w(\|F_o\| - \|F_c\|)^2$	$\Sigma w(\|F_o\| - \|F_c\|)^2$	$\Sigma w(\|F_o\| - \|F_c\|)^2$	$\Sigma w(\|F_o\| - \|F_c\|)^2$	$\Sigma w(\|F_o\| - \|F_c\|)^2$	$\Sigma w(\|F_o\| - \|F_c\|)^2$	$\Sigma w(\|F_o\| - \|F_c\|)^2$	$\Sigma w(\|F_o\| - \|F_c\|)^2$	$\Sigma w(\|F_o\| - \|F_c\|)^2$
weighting scheme	$\propto[\sigma^2(I) = 0.0009I^2]^{1/2}$	$\propto[\sigma^2(I) = 0.0009I^2]^{1/2}$	$\propto[\sigma^2(I) = 0.0009I^2]^{1/2}$	$\propto[\sigma^2(I) = 0.0009I^2]^{1/2}$	$\propto[\sigma^2(I) = 0.0009I^2]^{1/2}$	$\propto[\sigma^2(I) = 0.0009I^2]^{1/2}$	$\propto[\sigma^2(I) = 0.0009I^2]^{1/2}$	$\propto[\sigma^2(I) = 0.0009I^2]^{1/2}$	$\propto[\sigma^2(I) = 0.0009I^2]^{1/2}$	$\propto[\sigma^2(I) = 0.0009I^2]^{1/2}$
parameters refined	104	226	83	304	424	487	194	289	171	454
data/parameter ratio	3.52	6.03	9.76	8.56	4.80	6.41	8.85	7.26	7.56	8.22
unweighted agreement factor, R	0.068	0.053	0.039	0.062	0.051	0.078	0.051	0.041	0.062	0.042
weighted agreement factor, R_w	0.059	0.048	0.047	0.063	0.039	0.070	0.050	0.043	0.054	0.043
high peak in final difference map, e$^-$/Å^3	0.24[b]	0.21[b]	0.28 (Na1)	0.40 (C53)	0.27 (H24)	0.35 (C47)	0.37[b]	0.20 (N26)	0.47 (Fe1)	0.47 (Fe1)

[a] Full-matrix least-squares refinement. [b] Background. [c] −65 °C.

Scheme I

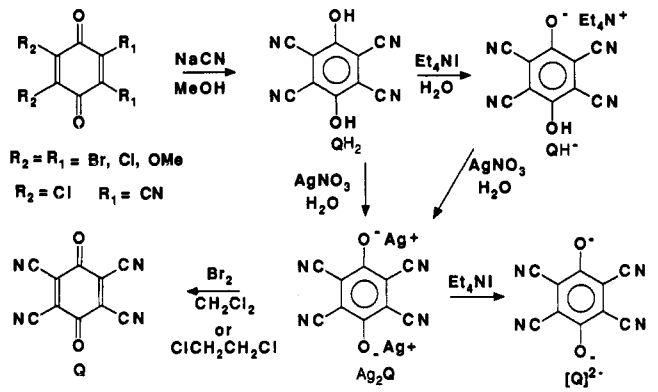

Table II. Representative Reversible One-Electron Reduction Potentials[a] for Strong Acceptors

acceptor[b]	$E^{0/-}$	$E^{-/2-}$
cyanil, **Q**	0.90	0.09[c,f]
DDQ	0.59	−0.25[f]
chloranil	0.05	−0.79[f]
$TCNQ(CN)_4$	1.31[d]	0.51[e]
$C_3[C(CN)_2]_3$	1.13[d]	0.34[e]
$C_4(CN)_6$	0.60	0.02[e]
$TCNQF_4$	0.53	0.02[e]
TCNQ	0.17	−0.37[e]
TCNE	0.15	−0.57[e]

[a] V vs SCE in MeCN {Pt electrode; 0.1 M $[n\text{-}Bu_4N][ClO_4]$}. [b] DDQ = 2,3-dichloro-5,6-dicyanobenzoquinone, TCNQ = 7,7,8,8-tetracyano-*p*-quinodimethane, $TCNQF_4$ = perfluoro-7,7,8,8-tetracyano-*p*-quinodimethane, $TCNQ(CN)_4$ = percyano-7,7,8,8-tetracyano-*p*-quinodimethane. [c] $[Q]^{2-}/[Q]^{3-}$ has a quasi-reversible reduction potential at −1.81 V. [d] The acceptor in the neutral form has not been isolated. [e] Ward, M. D. *Electroanal. Chem.* **1989**, *16*, 182. [f] This work.

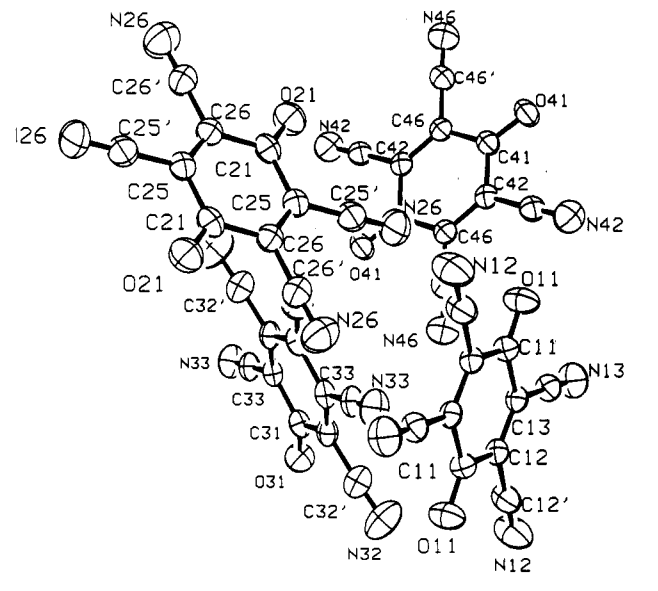

Figure 1. Atom labeling for cyanil, **Q**.

thracene and 2,3-dichloro-5,6-dicyanohydroquinone (H_2DDQ); thus, **Q** is a stronger hydrogen abstraction reagent than 2,3-dichloro-5,6-dicyanobenzoquinone (DDQ), the conventional reagent for this purpose.[23]

Crystal Structures. Cyanil, **Q**, crystallizes in the triclinic $P\bar{1}$ space group, and the asymmetric unit contains four molecules on different inversion centers. The atom labeling and a stereoview of the unit cell can be found in Figures 1 and 2, respectively. The bond distances are given in Table III. There are four independent cyanils in the unit cell, and these are in a tetrahedral arrangement such that each cyanil is surrounded by eight near neighbors. Close O···O interactions of 2.90 Å are present, but the

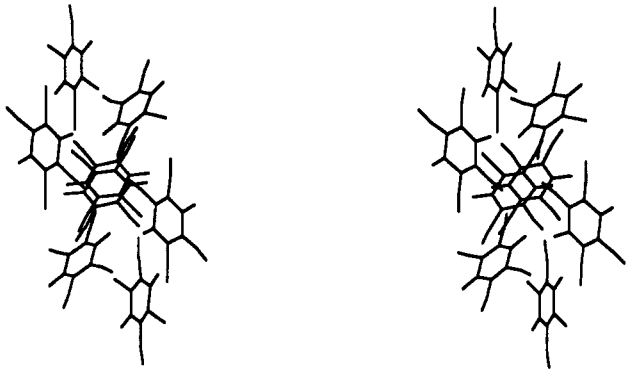

Figure 2. Stereoview of the unit for cyanil, **Q**.

Table III. Bond Distances, Å, for Q, QH_2, $[Fe(C_5Me_5)_2]^{+}[Q]^{-}$, $\{[Et_4N]^{+}\}_2[Q]_2^{2-}$, and $\{[(Ph_3P)_2N]^{+}\}_2[Q]^{2-}$

cyanil, Q			
O(11)–C(11)	1.202 (3)	C(13)–C(13′)	1.440 (4)
O(21)–C(21)	1.202 (3)	C(21)–C(25)	1.481 (4)
O(31)–C(31)	1.208 (3)	C(21)–C(26)[b]	1.499 (4)
O(41)–C(41)	1.206 (3)	C(25)–C(25′)	1.437 (4)
N(12)–C(12′)	1.132 (3)	C(25)–C(26)	1.336 (4)
N(13)–C(13′)	1.132 (3)	C(26)–C(26′)	1.429 (4)
N(26)–C(26′)	1.132 (4)	C(31)–C(32)	1.490 (4)
N(26)–C(25′)	1.131 (4)	C(31)–C(33)[c]	1.486 (4)
N(32)–C(32′)	1.134 (4)	C(32)–C(32′)	1.435 (4)
N(33)–C(33′)	1.135 (3)	C(32)–C(33)	1.340 (4)
N(42)–C(42′)	1.124 (3)	C(33)–C(33′)	1.435 (4)
N(46)–C(46′)	1.134 (3)	C(41)–C(42)	1.488 (4)
C(11)–C(12)	1.487 (3)	C(41)–C(46)[d]	1.483 (4)
C(11)–C(13)[a]	1.485 (4)	C(42)–C(42′)	1.447 (4)
C(12)–C(12′)	1.439 (4)	C(42)–C(46)	1.342 (3)
C(12)–C(13)	1.334 (3)	C(46)–C(46′)	1.435 (4)
tetracyano-*p*-hydroquinone, QH_2-dioxane			
O(1)–C(1)	1.332 (11)	C(1)–C(3)[e]	1.414 (14)
O(1)–H(1)	0.908 (83)	C(2)–C(2′)	1.517 (14)
N(2)–C(2′)	0.853 (14)	C(2)–C(3)	1.411 (14)
N(3)–C(3′)	0.842 (14)	C(3)–C(3′)	1.531 (15)
C(1)–C(2)	1.372 (13)		
$\{[Et_4N]^{+}\}_2[Q]_2^{2-}$			
O(1)–C(10)	1.242 (5)	C(11)–C(12)	1.387 (6)
O(2)–C(13)	1.231 (5)	C(11)–C(16)	1.439 (6)
N(16)–C(16)	1.138 (5)	C(12)–C(13)	1.468 (6)
N(17)–C(17)	1.127 (6)	C(12)–C(17)	1.436 (6)
N(18)–C(18)	1.138 (5)	C(13)–C(14)	1.470 (6)
N(19)–C(19)	1.144 (5)	C(14)–C(15)	1.381 (6)
C(10)–C(11)	1.457 (6)	C(14)–C(18)	1.442 (6)
C(10)–C(15)	1.456 (6)	C(15)–C(19)	1.434 (6)
$[Fe(C_5Me_5)_2]^{+}[Q]^{-}$			
O(1)–C(1)	1.226 (4)	C(3)–C(3′)	1.447 (4)
N(3)–C(3′)	1.132 (4)	C(5)–C(5′)	1.433 (4)
C(1)–C(2)	1.470 (4)	C(6)–C(6′)	1.442 (4)
C(2)–C(3)	1.366 (4)	N(2)–C(2′)	1.138 (4)
C(4)–C(5)	1.467 (4)	N(6)–C(6′)	1.138 (4)
O(4)–C(4)	1.233 (3)	C(2)–C(2′)	1.437 (4)
N(5)–C(5′)	1.142 (4)	C(3)–C(4)	1.459 (4)
C(1)–C(6)	1.455 (4)	C(5)–C(6)	1.377 (4)
$\{[(Ph_3P)_2N]^{+}\}_2[Q]^{2-}$			
O(1)–C(1)	1.268 (6)	C(1)–C(6)	1.434 (7)
N(1)–C(2′)	1.161 (7)	C(2)–C(2′)	1.383 (7)
N(6)–C(6′)	1.178 (7)	C(2)–C(6)[f]	1.414 (7)
C(1)–C(2)	1.418 (8)	C(6)–C(6′)	1.379 (8)

[a] $1-x, -y, 1-z$. [b] $-x, 1-y, 1-z$. [c] $-x, -y, -z$. [d] $1-x, 1-y, -z$. [e] $-x, 1-y, 1-z$. [f] $1-x, 1-y, 1-z$.

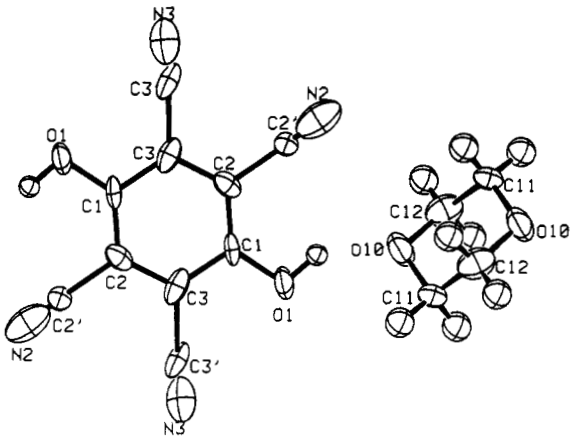

Figure 3. Atom labeling for tetracyanohydroquinone, QH_2-dioxane.

orientations of the C–O bonds are not consistent with bridging hydrogens (see below). Furthermore, there is no evidence of residual electron density at the positions expected for hydroxyl hydrogens. All other intermolecular contacts are ≥3.5 Å.

The geometry of cyanil has a quinone geometry with two short C=C bonds of 1.338 Å and four long C–C bonds of 1.488 Å in the ring. The C–O bonds are short and consistent with a C=O group and not with the presence of additional protons as noted above. The geometry is very similar to that of DDQ which has average values of r(C=C) = 1.342 Å, r(C–C) = 1.489 Å, and r(C=O) = 1.209 Å. The cyano groups have r(C–C) = 1.437 Å and r(C≡N) = 1.132 Å, again similar to the values of 1.455 and 1.135 Å found for DDQ.[24]

Tetracyanohydroquinone, QH_2, crystallizes as the dioxane solvate in the monoclinic $P2_1/c$ space group, and the asymmetric unit contains half of the molecules which are related by different inversion centers. The atom labeling can be found in Figure 3. The cyanobenzene layers consist of herringbone arrays with a stacking distance of 3.36 Å. The arrays are held together by OH···O hydrogen bonds between the OH groups on QH_2 and O on the dioxane, r[O(10)–H(1)] = 1.78 Å as compared to r[O(1)–H(1)] = 0.91 Å.

The ring geometry has a more aromatic structure than found for **Q** with two C–C bond distances of 1.372 Å and four C–C bond distances of 1.413 Å. The C–O bond is elongated by 0.13 Å as compared to **Q**. The positions of the C≡N groups are not well-determined with r(C–C) too long and r(C≡N) far too short. The low data/parameter ratio plus poor crystal quality probably accounts for the unreasonably short C≡N bonds.[25]

$\{[Et_4N]^+\}_2[Q]_2^{2-}$ crystallizes in the monoclinc $P2_1/n$ space group, and the asymmetric unit contains a cation and anion on general positions. The atom labeling and a stereoview of the unit cell can be found in Figures 4 and 5, respectively. The anion form chains of $[Q]_2^{2-}$ dimers, Figure 6a. The anion bond distances are given in Table III. For convenience a mean plane is defined by the four ring carbons bound to nitriles. Each of these ring carbons deviates from the mean plane by 0.003 Å, whereas the carbonyl carbons deviate on average 0.06 Å from this mean plane. The cyanocarbons, nitrogens, and oxygens respectively deviate on average 0.08, 0.14, and 0.12 Å from this mean plane. Thus, the anion is folded with respect to a plane containing the carbonyls. The dimer dianions form 1D chains with the closest intradimer separations being 2.80 (C···O) and 2.89 (C···O) Å. The mean plane (defined by the four ring-C–CN's) intra- and interdimer separations are 2.87 and 3.48 Å, respectively. The respective centroid (defined by the four ring-C–CN's)-to-centroid distances are 3.55 and 3.88 Å. This behavior where the anions bend and couple to form strongly interacting pairs is similar to certain $[TCNE]_2^{2-}$ salts;[26] however, unlike $[TCNE]_2^{2-}$ each half of the $[Q]_2^{2-}$ dimer is slipped with respect to each other.

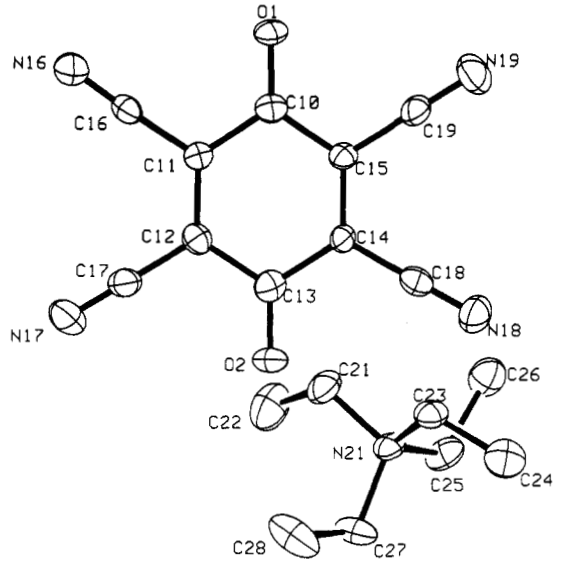

Figure 4. Atom labeling of $\{[Et_4N]^+\}_2[Q]_2^{2-}$.

The geometry of the monomer of $[Q]_2^{2-}$ shows C–O bonds longer by 0.03 Å and four C–C ring bonds shorter by 0.025 Å as compared to **Q**. The largest change is a lengthening of the ring C=C bonds by 0.046 Å in the monomer of $[Q]_2^{2-}$. The remaining C–CN and C≡N bonds do not change as compared to **Q**.

$\{[Fe(C_5Me_5)_2]^{\bullet+}\}_2[Q]_2^{2-}$ crystallizes in the monoclinic $P2_1/n$ space group, and the asymmetric unit contains a cation and anion on general positions. The atom labeling and a stereoview of the unit cell can be found in Figures 7 and 8, respectively. The anion form chains of $[Q]_2^{2-}$ dimers, Figure 6b. The anion bond distances are given in Table III. Again for convenience a mean plane is defined by the four ring-C bound to cyanides. Each of the these ring carbons deviates from the mean plane by 0.002 Å, whereas the carbonyl carbons average 0.02 Å out of this mean plane. The cyano carbons, nitrogens, and oxygens deviate an average of 0.04, 0.07, and 0.10 Å, respectively, from this mean plane. Again, the anion is folded with respect to a plane containing the carbonyls, but the folding is not as severe as observed for the $[Et_4N]^+$ salt (vide supra). As observed for the $[Et_4N]^+$ salt, the anions form 1D chains with closest interanion separations of 2.91 (C···O) and 2.94 (C···C) Å. The mean plane (defined by the four ring-C–CN's) intra- and interdimer separations are 2.88 and 3.30 Å, respectively. The respective centroid (defined by the four ring-C–CN's)-to-centroid distances are 3.55 and 3.86 Å.

(24) Miller, J. S.; Krusic, P. J.; Dixon, D. A.; Reiff, W. M.; Zhang, J. H.; Anderson, E. C.; Epstein, A. J. *J. Am. Chem. Soc.* **1986**, *108*, 4459.

(25) Refinement of an isonitrile model yields a slightly lower $R = 0.066$ and $R_w = 0.058$ and more reasonable thermal parameters, but such a structure is not in agreement with the chemistry.

(26) Miller, J. S.; O'Hare, D. M.; Chakraborty, A.; Epstein, A. J. *J. Am. Chem. Soc.* **1989**, *111*, 7853.

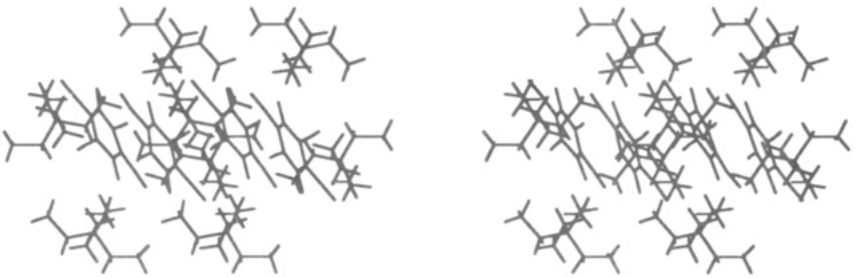

Figure 5. Stereoview of the unit cell for $\{[Et_4N]^+\}_2[\mathbf{Q}]_2^{2-}$.

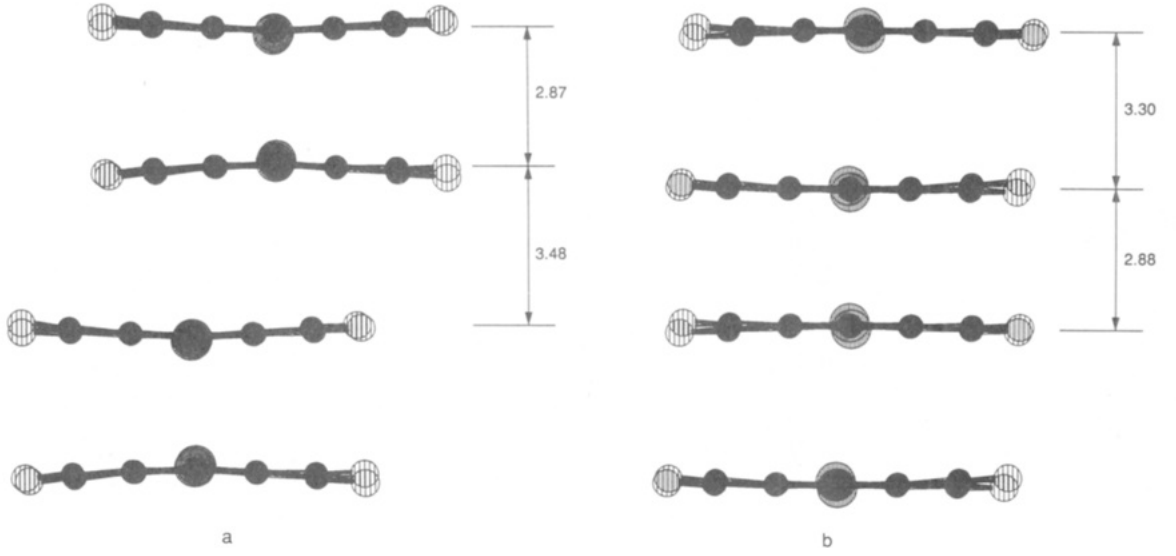

Figure 6. Chain segment of $[\mathbf{Q}]_2^{2-}$ in $\{[Et_4N]^+\}_2[\mathbf{Q}]_2^{2-}$ (a) and $\{Fe(C_5Me_5)_2]^{\bullet+}\}_2[\mathbf{Q}]_2^{2-}$ (b).

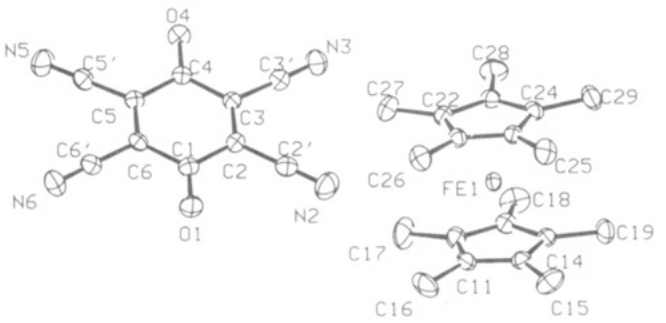

Figure 7. Atom labeling for $\{[Fe(C_5Me_5)_2]^{\bullet+}\}_2[\mathbf{Q}]_2^{2-}$.

The anions form 1D chains with each cyanil stack surrounded by six $[Fe(C_5Me_5)_2]^{\bullet+}$ chains. The cyanils pair within a stack resulting in separations between cyanils of 2.84 and 3.27 Å, similar to the interactions found in the $[NEt_4]^+$ salt.

The structures of the pair of dimer dianions are quite similar with only the C–CN distances differing by significant amounts. The four ring-C–C bonds are the same in the two structures and the CO and ring-CC bonds show smaller changes from those in the $[Fe(C_5Me_5)_2]^{\bullet+}$ salt.

A number of structures of $[\mathbf{Q}]^{2-}$ plus a proton were determined. These structures generally have protons binding the dianions together in complicated arrays. The cyanil portion often sits on a special position and usually does not exhibit the asymmetry expected for an isolated $[\mathbf{QH}]^-$ (vide infra).

$\{[(\mathbf{Ph_3P})_2\mathbf{N}]^+\}_2[\mathbf{Q}]^{2-}$ crystallizes in the monoclinic $P2_1/c$ space group, and the asymmetric unit contains a half anion on an inversion center and a cation located at a general position. The atom labeling can be found in Figure 9. The anion bond distances are given in Table III. The C–O bond distances is shorter than found for other "dianion" structures, i.e., $[H]^+[\mathbf{Q}]^{2-}$, consistent with the absence of hydrogen bonding in the structure. The ring-C–C bond distances [1.414 (7)–1.434 (7) Å (averaging 1.422 Å)] are consistent with a dianion with an aromatic ring. The C–CN bond distances are also quite short consistent with the presence of valence bond structures with >C=C=N$^-$ character. These results are all consistent with the formation of a isolated dianion unperturbed by hydrogen bonding via the oxygens.

$[\mathbf{Fe(C_5Me_5)_2}]^{\bullet+}[\mathbf{H}]^+[\mathbf{Q}]^{2-}$ crystallizes in the monoclinic $C2/c$ space group, and the asymmetric unit contains half of a cation on an inversion center ($^1/_4$, $^1/_4$, 0) and half of an anion on an inversion center at the origin. The atom labeling and a stereoview of the unit cell are found in Figures 10 and 11, respectively. The anion bond distances are given in Table IV. The cyanil dianions are bonded by H^+ between the two oxygens with O–H distances of 1.29 Å. The O···O distances is thus quite short, 2.58 Å. The CO distances (1.309 Å) are much longer than those in the isolated monoanions. The ring-C–C bonds are approximately equal (1.399, 1.402, and 1.414 Å) consistent with a benzenoid structure for the ring. These results suggest that the negatively charged moiety is best described as $[\mathbf{Q}]^{2-}$.

$[\mathbf{Me_4N}]^+[\mathbf{H}]^+[\mathbf{Q}]^{2-}$ crystallizes in the monoclinc $P2_1/n$ space group, and the asymmetric unit contains two half anions which are related by different inversion centers. The cation is located at a general position. The atom labeling and a stereoview of the unit cell can be found in

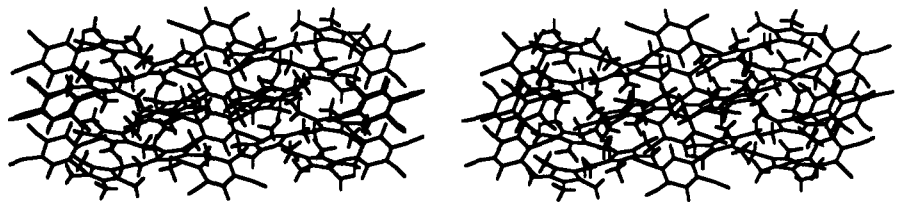

Figure 8. Stereoview of the unit cell for $\{[Fe(C_5Me_5)_2]^{\bullet+}\}_2[Q]_2^{2-}$.

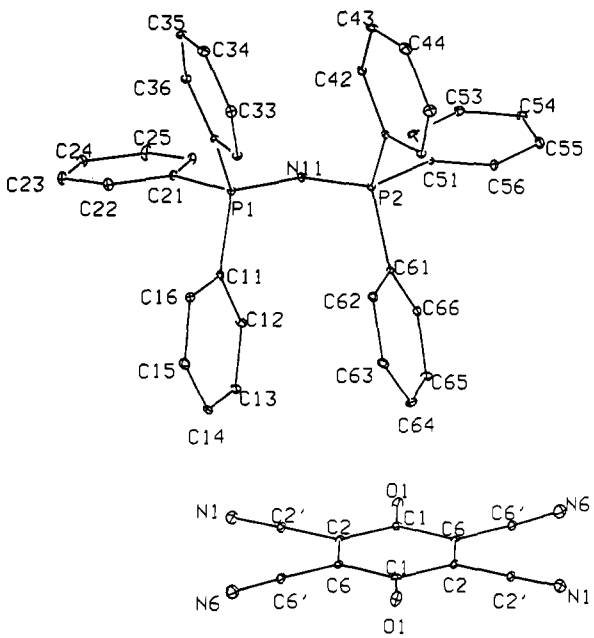

Figure 9. Atom labeling for $\{[(Ph_3P)_2N]^+\}_2[Q]^{2-}$.

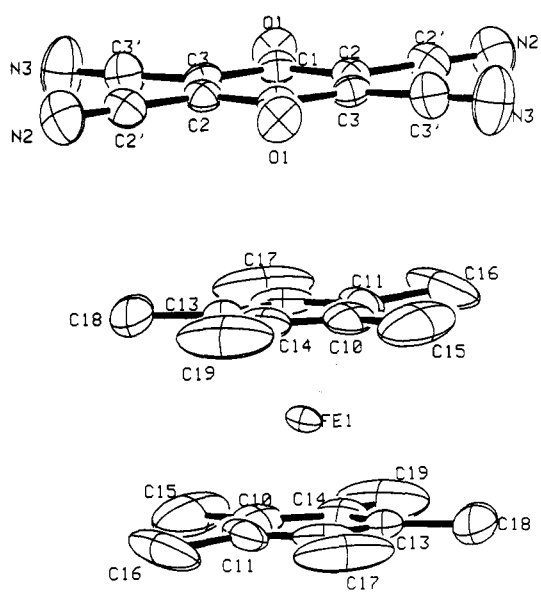

Figure 10. Atom labeling for $[Fe(C_5Me_5)_2]^{\bullet+}[H]^+[Q]^{2-}$.

Figures 12 and 13, respectively. The anion bond distances are given in Table IV. The O atoms are connected by a proton with a short O···O distance of 2.43 Å. The proton is apparently displaced towards one cyanil group, but the large thermal parameters and errors in the O–H bond distances do not conclusively show this. The C–O bonds are again long (1.310 and 1.320 Å). The six ring-C–C bonds are very similar (1.400–1.411 Å) and show the rings to be benzene-like. Again the structure is best described as $[Q]^{2-}$connected by protons.

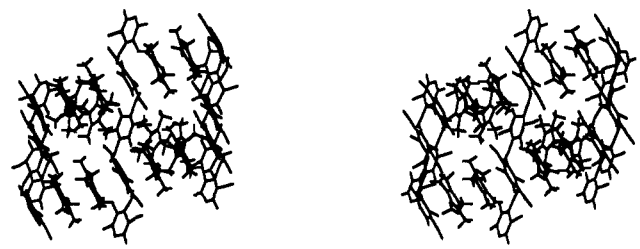

Figure 11. Stereoview of the unit cell for $[Fe(C_5Me_5)_2]^{\bullet+}$-$[H]^+[Q]^{2-}$.

$Na^+[H]^+[Q]^{2-}$ crystallizes in the triclinic $P\bar{1}$ space group, and the asymmetric unit contains half of the anion which is related to itself by an inversion center. The Na^+ is located at the origin and at the inversion center. The atom labeling and a stereoview of the unit cell can be found in Figures 14 and 15, respectively. The bond distances are given in Table IV. The geometry of the anion closely resembles that of $[Q]^{2-}$ with strong bonds to H^+ and Na^+. The ring-CC bond lengths are similar to each other with the C_2–C_3 bonds (the original C=C bonds) being 0.018 Å shorter than the remaining four bonds. The exocyclic C–CN bonds average 1.441 Å. The protons were refined in half-weighted positions near the O atoms. This two-site refinement suggests that the H^+ is in a very mobile position. Each Na^+ is coordinated to six different cyanil moieties and there are two O···Na interactions of 2.46 Å and four Na···N interactions also averaging 2.46 Å. Thus, the anion chains are held together by H^+ bridging the O^- groups as well as Na^+ interactions.

$[Et_4N]^+[QH]^-$ crystallizes in the monoclinic $P2_1/c$ space group and, the asymmetric unit contains two half anions which are related by different inversion centers, an anion in a general position, and two cations in general positions. The atom labeling and a stereoview of the unit cell can be found in Figures 16 and 17, respectively. The anion bond distances are given in Table IV. The structure of the anion on a general position resembles $[QH]^-$ but is quite distorted. The other two anions are closer to strongly H^+-bonded $[Q]^{2-}$ moieties, but are also quite distorted. The distortions in all three anions can be seen not only in the rings but also in the exocyalic C–CN bonds. The disordered $[NEt_4]^+$ group may be affecting the determination of the anion structures. The structure is held together by strong H^+ bonds to the oxygens. The short O···O interaction distances are r(O14–O11) = 2.56 Å and r(O21–O31) = 2.38 Å. Two interacting chains are formed, one involving the anions in a general position and one involving those on the inversion centers.

$[n\text{-}Bu_4N]^+[QH]^-$ crystallizes in the monoclinic $C2/c$ space group, and the asymmetric unit contains two half anions: one on an inversion center and the second on a 2-fold axis. The cation is located at a general position. The atom labeling and a view of a layer can be found in Figures 18 and 19, respectively. The anion bond distances are given in Table IV. The anion on the 2-fold axis can

Table IV. Bond Distances, Å, for $Na^+[H]^+[Q]^{2-}$, $[Me_4N]^+[H]^+[Q]^{2-}$, $[n\text{-}Bu_4N]^+[QH]^-$, $[Fe(C_5Me_5)_2]^{\cdot+}[H]^+[Q]^{2-}$, and $[Et_4N]^+[QH]^-$

$Na^+[H]^+[Q]^{2-}$		$[Me_4N]^+[H]^+[Q]^{2-}$		$[n\text{-}Bu_4N]^+[QH]^-$	
Na(1)–O(1)[a]	2.461 (2)	O(1)–C(1)	1.310 (3)	O(1)–C(1)	1.324 (4)
Na(1)–N(2)[b]	2.447 (2)	O(2)–C(4)	1.320 (3)	O(10)–C(10)	1.350 (6)
Na(1)–N(3)[c]	2.468 (2)	O(1)–H(1)	1.148 (52)	O(11)–C(13)	1.253 (5)
O(1)–C(1)	1.309 (2)	O(2)–H(1)	1.283 (52)	O(1)–H(1)	1.528 (76)
O(1)–H(1)	0.785 (61)	N(2)–C(2′)	1.130 (3)	O(10)–H(1)	1.198 (77)
N(2)–C(2′)	1.141 (3)	N(3)–C(3′)	1.135 (3)	N(4)–C(4)	1.147 (5)
N(3)–C(3′)	1.138 (3)	N(5)–C(5′)	1.135 (4)	N(5)–C(5)	1.123 (5)
C(1)–C(2)	1.411 (3)	N(6)–C(6′)	1.142 (3)	N(16)–C(16)	1.145 (4)
C(1)–C(3)[e]	1.411 (3)	C(1)–C(2)	1.411 (4)	N(17)–C(17)	1.145 (4)
C(2)–C(2′)	1.440 (3)	C(1)–C(3)	1.402 (4)	C(1)–C(3)	1.417 (5)
C(2)–C(3)	1.394 (3)	C(2)–C(2′)	1.446 (4)	C(2)–C(3)[h]	1.418 (5)
C(3)–C(3′)	1.442 (3)	C(2)–C(3)[f]	1.404 (3)	C(2)–C(4)	1.409 (5)
H(1)–H(1)[d]	0.926 (117)	C(3)–C(3′)	1.439 (4)	C(3)–C(5)	1.435 (6)
		C(4)–C(5)	1.407 (3)	C(10)–C(11)	1.402 (4)
		C(4)–C(6)	1.400 (4)	C(11)–C(12)	1.398 (4)
		C(5)–C(5′)	1.431 (4)	C(11)–C(16)	1.438 (5)
		C(5)–C(6)[g]	1.406 (4)	C(12)–C(13)	1.438 (4)
		C(6)–C(6′)	1.439 (4)	C(12)–C(17)	1.437 (5)

$[Fe(C_5Me_5)_2]^{\cdot+}[H]^+[Q]^{2-}$		$[Et_4N]^+[QH]^-$			
O(1)–C(1)	1.307 (6)	O(11)–C(11)	1.234 (7)	C(15)–C(15′)	1.443 (8)
O(1)–H(1)	1.289 (7)	O(14)–C(14)	1.330 (7)	C(15)–C(16)	1.350 (8)
N(2)–C(2′)	1.139 (7)	O(21)–C(21)	1.356 (9)	C(16)–C(16′)	1.460 (10)
N(3)–C(3′)	1.136 (8)	O(31)–C(31)	1.355 (9)	C(21)–C(22)	1.393 (9)
C(1)–C(2)	1.399 (8)	N(12)–C(12′)	1.176 (7)	C(21)–C(26)	1.303 (12)
C(1)–C(3)[g]	1.414 (8)	N(13)–C(13′)	1.143 (8)	C(22)–C(22′)	1.385 (12)
C(2)–C(2′)	1.431 (8)	N(15)–C(15′)	1.114 (8)	C(22)–C(26)[i]	1.477 (11)
C(2)–C(3)	1.402 (8)	N(16)–C(16′)	1.157 (8)	C(26)–C(26′)	1.489 (11)
C(3)–C(3′)	1.446 (9)	N(22)–C(22′)	1.139 (10)	C(31)–C(32)	1.408 (9)
		N(26)–C(26′)	1.137 (9)	C(31)–C(36)	1.307 (12)
		N(32)–C(32′)	1.141 (11)	C(32)–C(32′)	1.383 (12)
		N(36)–C(36′)	1.146 (10)	C(32)–C(36)[j]	1.468 (11)
		N(41)–C(41)	1.510 (5)	C(36)–C(36′)	1.487 (12)
		C(11)–C(12)	1.509 (9)	C(11)–C(16)	1.435 (8)
		C(12)–C(12′)	1.389 (8)	C(12)–C(13)	1.359 (9)
		C(13)–C(13′)	1.502 (10)	C(13)–C(14)	1.385 (7)
		C(14)–C(15)	1.432 (9)		

[a] $x, -1 = y, z$. [b] $1 = x, -1 = y, z$. [c] $1 = x, -1 = y, -1 = z$. [d] $1 - x, 1 - y, -z$. [e] $1 - x, 1 - y, 1 - z$. [f] $1 - x, -y, 1 - z$. [g] $-x, -y, -z$. [h] $-x, -y, 1 - z$.

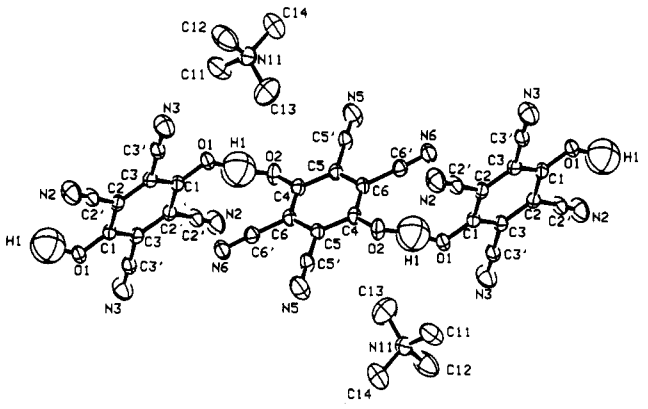

Figure 12. Atom labeling for $[Me_4N]^+[H]^+[Q]^{2-}$.

best be described as $[QH]^-$ with one short C–O and one long C–O bond (see below). The other anion has more of a $[Q]^{2-}$ structure (equivalent C–C ring bonds) and longer C–O bonds. The O atoms in the latter are involved in strong hydrogen bonding. There is a strongly bonded hydrogen to the $[QH]^-$ which is disordered showing up in two equivalent positions and helping to hold the anion chains together. The structure is characterized by only one short O···O interaction of 2.70 Å.

Hydrogen Bonding. A characteristic structural feature of the protonated cyanil anion salts is the presence of strong intermolecular hydrogen bonding with O···O separations less than 2.5 Å as observed for the $[Me_4N]^+$, $[Et_4N]^+$, and Na^+ salts (Table V). The degree of protonation varies with counterion with examples of both $[QH]^-$ and $[H]^+[Q]^{2-}$ being observed. The O···O distance in the $[Me_4N]^+$ salt, as far as we can determine, is the shortest reported for an an organic system with intermolecular hydrogen bonding.[27] Intermolecular hydrogen bonding in inorganic systems frequently have shorter O···O separations, e.g., $[H_3O_2]^-$ (2.29 Å)[27c] and $[H_5O_2]^+$ (2.41 to 2.45 Å).[27a] [For comparison F···F separations in $[HF_2]^-$ salts range from 2.26 to 2.28 Å depending upon the cation.][27a] Examples where O···O separations < 2.45 Å exist are Speakman salts (carboxylate/carboxyl charged pairs),[27a,d] β-diketones,[27b] and bis(dioximato)metal complexes.[27a] The infrared δ(OH) absorption for strong hydrogen bonds occurs below 1600 cm^{-1} and is very broad.[27a] Thus, it is not surprising that we were unable to observed infrared features assignable to this for the protonated cyanil anion salts.

Calculated Geometries. The calculated geometry of cyanil (Table VI) agrees quite well with the experimental one. The C=O bond is calculated to be shorter than observed by 0.02 Å as would be expected for a Hartree–

(27) (a) Emesley, J. *Chem. Soc. Rev.* **1980**, *9*, 91. (b) Emesley, J. *Struct. Bond. (Berlin)* **1984**, *57*, 147. (c) A-Dari, K.; Raymond, K. N.; Freyberg, D. P. *J. Am. Chem. Soc.* **1979**, *101*, 3688. (d) Speakman, J. C. *Struct. Bond (Berlin)* **1972**, *12*, 141.

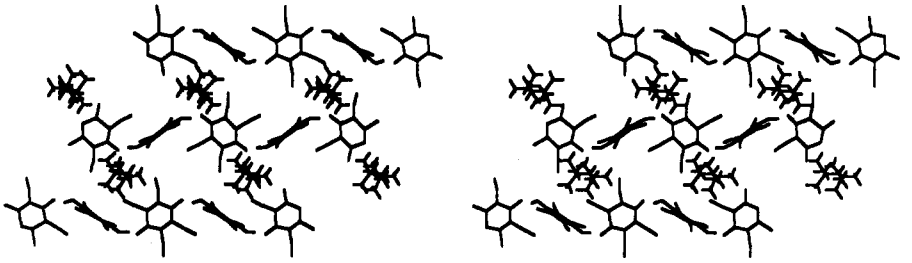

Figure 13. Stereoview of the unit cell for $[Me_4N]^+[H]^+[Q]^{2-}$.

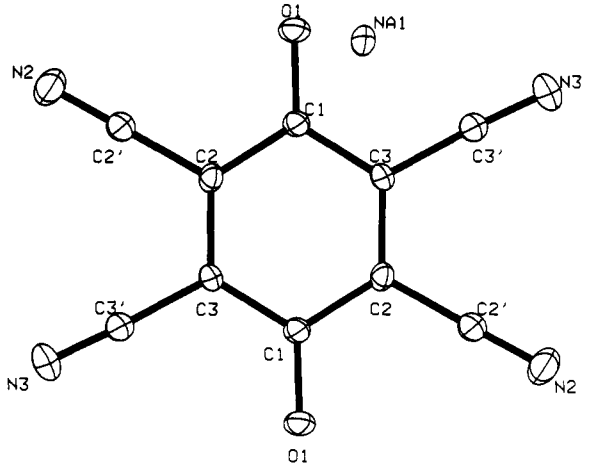

Figure 14. Atom labeling for $Na^+[H]^+[Q]^{2-}$.

Fock calculation. The four ring C–C bonds are calculated to be too long by 0.015 Å which is unusual for this level of calculation. Consistent with previous work, the CN bond lengths are longer than the experimental ones.[28] This is due to the difficulty of measuring the C≡N bond by X-ray methods. The remaining calculated distances are quite similar to the experimental ones. The calculated total energies are presented as supplementary materials.

The calculated structure of the anion agrees quite well with the average experimental one (Table VI). The largest differences are the exocyclic C–CN and C≡N bond lengths which are both calculated to be longer than the experimental ones.

The calculated structure of the dianion is in reasonable agreement with the experimental structure of the $\{[(PPh_3)_2N]^+\}_2[Q]^{2-}$ salt (Table VI). The calculated C–O and ring C–C distances are in good agreement with the experimental values. The only major differences are found for the C–CN bond distances where the experimental value is shorter by 0.06 Å. All of the ring C–C bonds are longer than those calculated for benzene (1.391 Å), and the ring is more asymmetric than the observed structure. The central $C_2C_1C_2$ angle decreases as charge is added to the system, and the other angles show smaller effects. The C–CN and CN bonds show little effect of adding the two negative charges.

The calculated structure obtained by addition of two protons (Table VII) is more like that of the observed dianion with strong H^+ bridges. The ring C–C bonds are all essentially equal as experimentally observed. The C–O bond distance is comparable to that found for QH_2 but is longer than the distance found for the proton bound dimer dianions. The ring bond angles are all near 120°. The COH bond angle is larger than tetrahedral, 113.4°. These results show that the experimental structure for the proton bound dimer dianions has more of this valence bond structure than it does of the isolated dianion structure.

Addition of a single proton leads to a very asymmetric anion. The calculated structure is slightly nonpolar (Table VIII). The C–O distances show a large difference of 0.14 Å. This leads to significant differences in the C–C ring bonds which range from 1.386 to 1.454 Å. These results clearly show that there are no completely isolated $[QH]^-$ structures in the crystal structures as we never observe this degree of asymmetry in the structure.

Charge Distributions. The charge distributions (Table IX) for cyanil show a polar C–O bond and a reverse polarized C≡N group (C negative; N positive) at the DZ + $D_{c,o}$ level. Addition of a negative charge leads to an increase in the polarity of the C–O bond. The C≡N bond is now polarized with the nitrogen negatively charged. Addition of a second charge leads to increased polarity in the CO and CN bonds.

Addition of two protons leads to a decrease in the anionic character on oxygen if the very polar O–H bond is accounted for by adding the H charge to the O. This leads to a decrease in the polarity of the C–O bond. The C≡N bonds still show a reverse polarization. If only one proton is added, the O^- becomes slightly more negative than in the dianion and the O with the proton becomes neutral after accounting for the charge on the hydrogen even though the C–O bond is still polarized toward the O. The polarity of the C≡N bonds is small with the C11–N and C12–N bonds of opposite polarity as compared to the C9–N and C10–N bonds.

Spectroscopic Properties. Vibrational. The various forms of $[Q]^n$ exhibit characteristic ν(C≡N) vibrational spectra (Table X). Compared to **Q**, the ν(C≡N) transition in $[Q]^-$ exhibits a slight blue shift with respect to the lower frequency stretch. For the isolated $[Q]^{2-}$ ion both of the absorptions are red shifted relative to **Q** as expected. For the salts where a H^+ is present with $[Q]^{2-}$, the ν(C≡N) absorptions show a pronounced blue shift. The $[QH]^-$ stretches are similar to those in $[H]^+[Q]^{2-}$ shifts, whereas for QH_2 the ν(C≡N) absorptions show a significant blue shift as compared to **Q**. A surprising result is the lack of a significant red shift and even a blue shift observed for the ν(C≡N) absorptions for the compounds derived from monoanions or dianions containing protons as compared to **Q**. This is in contrast to what is observed in other cyanocarbons and their anions and dianions. In these latter compounds the C≡N stretches exhibit a red shift consistent with some component of the >C=C=N⁻ resonance structure. For example, for $[DDQ]^n$ the ν(C≡N) stretches shift from 2234 and 2246 cm^{-1} for $n = 0$, to 2217 cm^{-1} for $n = 1-$, and to 2187 and 2200 cm^{-1} for $n = 2-$.[29]

(28) Dixon, D. A.; Calabrese, J. C.; Miller, J. S. *J. Chem. Phys.* **1989**, *93*, 2284. Miller, J. S.; Calabrese, J. C.; Dixon, D. A. *J. Chem. Phys.* **1991**, *95*, 3139.

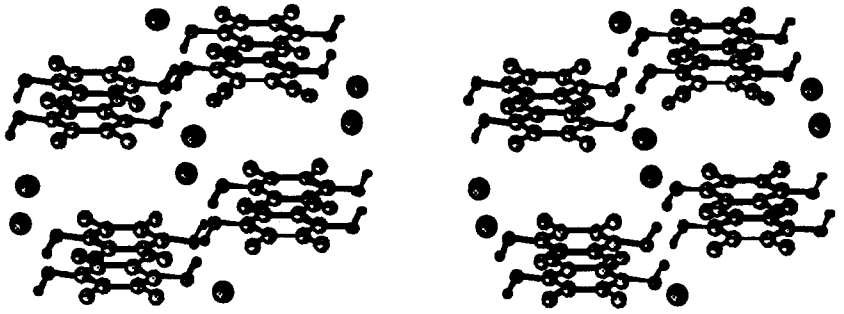

Figure 15. Stereoview of the unit cell for $Na^+[H]^+[Q]^{2-}$.

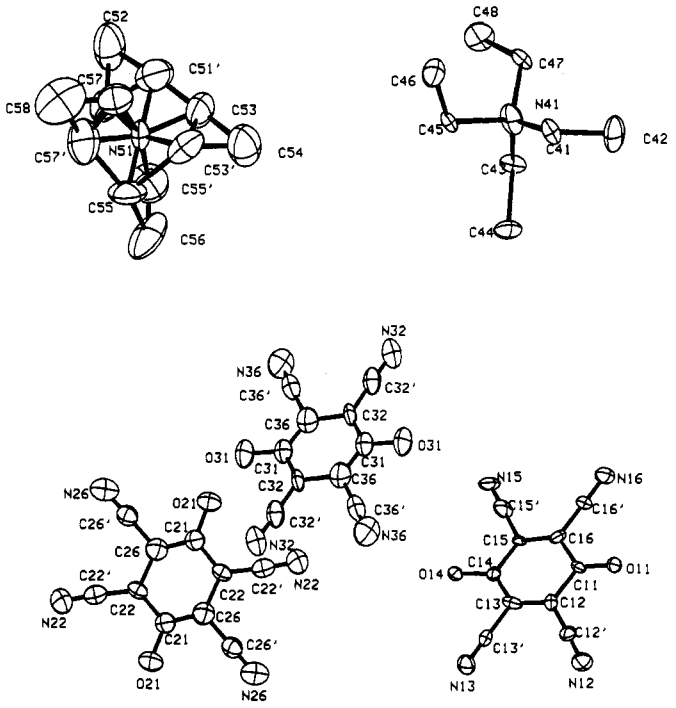

Figure 16. Atom labeling for $[Et_4N]^+[QH]^-$. The disordered cation can be found in the lower left.

Only for the isolated $[Q]^{2-}$ is the expected red-shift in the ν(C≡N) observed. The calculations predict a red-shift for the anion, dianion, and the protonated forms of $[Q]^{2-}$. This is in agreement with what is observed for DDQ, but not observed for **Q** with the exception of isolated $[Q]^{2-}$. For $[Q]_2^{2-}$ two ν(C≡N) transitions are observed as compared to one transition for $[Q]^{\bullet-}$. In comparison, for $[TCNE]_2^{2-}$ three ν(C≡N) transitions are observed in the IR as compared to the two transitions observed for $[TCNE]^{\bullet-}$.[26]

The observed Raman spectrum for QH_2 shows four ν(C≡N) absorption in contrast to the two predicted for a C_{2h} molecule. The two higher energy bands are inconsistent with the calculated values (vide infra). For $Na^+[H]^+[Q]^{2-}$ there are two strong Raman bands (~2240 cm^{-1}) and a weaker one (~2200 cm^{-1}). The Raman spectrum of the $[n\text{-}Bu_4N]^+$ salt has three Raman bands between 2200 and 2240 cm^{-1} just as three IR-active bands between 2207 and 2231 cm^{-1} were observed.

Calculated Vibrational Frequencies. The calculated vibrational spectra for the cyano stretches are given in Table X with the remainder presented as supplementary material. Comparison of the cyano bands for **Q** shows that the two observed IR bands are calculated to be at too high a frequency. A scale factor of 0.88 brings the calculated bands into reasonable agreement. This scaling factor was also required for the ν(C≡N) stretches in $[TCNE]^{2-}$.[30] The calculated splitting is somewhat smaller than the observed one. The ν(C≡N) stretches for QH_2 are expected to be slightly lower than those of **Q**. The opposite is experimentally observed. Use of the above scale factor gives values for QH_2 that are low by ~50 cm^{-1} which is somewhat surprising. Similarly the calculations suggest that the ν(C≡N) stretches for $[Q]^{2-}$ are about 90 cm^{-1} below that for **Q** as compared to the experimental results which have a red shift of ~50 cm^{-1}. For $[Q]^{\bullet-}$ the ν(C≡N) stretches are predicted to be 30–40 cm^{-1} below those of **Q** in contrast to the experimental results. For $[QH]^-$ the calculations predict four observable ν(C≡N) bands with a splitting of ~35 cm^{-1} between the highest and lowest absorptions. Again these are predicted to be less than those in **Q**, in contrast to the experimental observations. The lower frequency transitions should be more intense. The crystal structure of the $[n\text{-}Bu_4N]^+[QH]^-$ salt shows the presence of both $[QH]^-$ and $[Q]^{2-}$ moieties. Thus, it is not surprising that the Raman spectrum has three absorbances with one frequency lower than the lowest value for **Q**.

From the observed b_{3u} IR absorption (1689 cm^{-1}) of **Q** we calculate a scale factor of 0.84 for the ν_{CO} stretch. The C–O stretches in **Q** are only shifted to the red by 167 (a_{1g}) and 264 (b_{3g}) cm^{-1} for $[Q]^{\bullet-}$ and 264 (a_g) and 376 (b_u) cm^{-1} for $[Q]^{2-}$. In QH_2 the shifts are 227 (a_g) and 379 (b_u) cm^{-1}. For $[QH]^-$, the shifts are 233 and 289 cm^{-1}.

Electronic Absorption Spectra. The electronic absorption spectra for these species show a number of interesting features, Table XI, Figure 20. The calculated orbital energies are given in Table XII. The first transition in cyanil is at 27 000 cm^{-1}. The HOMO (b_{3g}) → LUMO (b_{2g}) transition is forbidden by symmetry based on the orbital ordering calculated with the DZ + $D_{c,o}$ basis set. The first observed transition can then be assigned to the NHOMO (b_{1u}) → LUMO transition which is symmetry allowed. The second transition has one resolved vibrational transition of 1270 cm^{-1} and can be assigned as the HOMO → NLUMO (a_u) transition. We note that these transitions are all $\pi \rightarrow \pi^*$ transitions, not the $n \rightarrow \pi^*$ transitions that might be expected for the carbonyls. The STO-3G basis set has a different ordering of the orbitals and gives a different set of assignments. At the STO-3G level the HOMO → LUMO transition is allowed by symmetry; thus, the first transition would be assigned to this. Both NHOMO → LUMO and HOMO → NLUMO

(29) Miller, J. S.; Dixon, D. A. *Science* **1987**, *235*, 871.

(30) Dixon, D. A.; Miller, J. S. *J. Am. Chem. Soc.* **1987**, *109*, 3656.

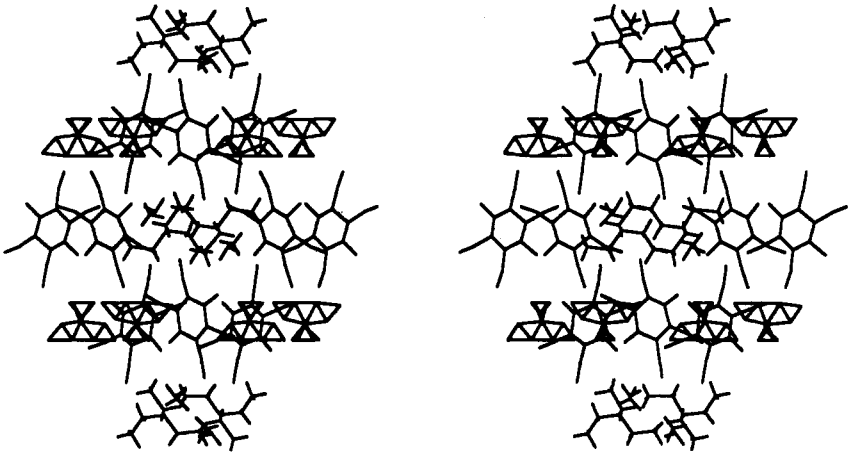

Figure 17. Stereoview of the unit cell for $[Et_4N]^+[QH]^-$. The three-membered rings belong to the disordered cations.

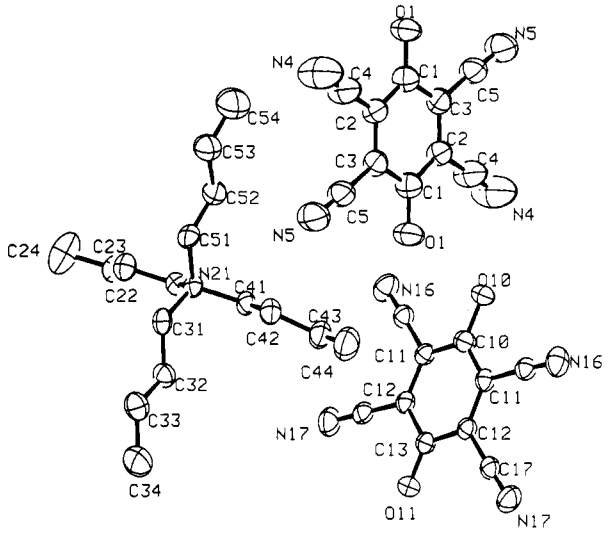

Figure 18. Atom labeling for $[n\text{-}Bu_4N]^+[QH]^-$.

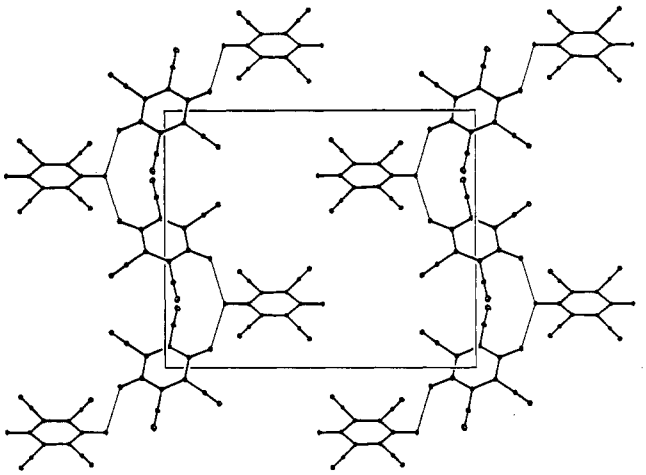

Figure 19. Hydrogen bonded layer of $[n\text{-}Bu_4N]^+[QH]^-$.

transitions are symmetry forbidden at the STO-3G level, and the next observed transition is either the NHOMO → NLUMO or some other occupied orbital to LUMO transition.

For $[Q]^{\bullet-}$, there are three transitions at low to medium energy as opposed to the single transition observed for **Q**. The first absorption shows a vibrational band of ~1850 cm^{-1} (similar to that of a $\nu(C{\equiv}O)$ stretch) between the peak and the shoulder. The next band shows two vibrational transitions at 1550 and 1460 cm^{-1}, which could be the C=C stretches. We have previously discussed the UV–vis spectrum of $[DDQ]^n$, n = 0, 1–, 2– in detail. We suggested that the low-energy transitions of the anion involved transitions among the occupied orbitals including the SOMO (the LUMO of **Q** by addition of an electron).[24] This leads to a decrease in the transition energy. We can apply the same model here. At the DZ + $D_{c,o}$ level, the orbitals have the same energy ordering as for **Q**. Thus the lowest energy transition cannot be assigned to the NHOMO (b_{3g}) → SOMO (b_{2g}) transition of the occupied orbitals as found in DDQ.[24] However, the NHOMO in **Q** is found to be close in energy to the HOMO. Since the transition from this orbital (2NHOMO, b_{1u}) to the SOMO is symmetry allowed, we assign the lowest observed transition to this. The next transition can probably be assigned to the SOMO → LUMO (a_u) transition which is symmetry allowed. At the STO-3G level, we would assign the lowest energy transition as being due to the NHOMO → SOMO transition which is symmetry allowed.

Table V. Short O···O Intermolecular Distances, Å, for $[QH]^-$ and $[H]^+[Q]^{2-}$ Compounds

compound	r(O···O), Å
$Na^+[H]^+[Q]^{2-}$	2.48
$[NMe_4]^+[H]^+[Q]^{2-}$	2.43
$[Fe(C_5Me_5)_2]^{\bullet+}[H]^+[Q]^{2-}$	2.58
$[NEt_4]^+[QH]^-$	2.38,2.56
$[n\text{-}NBu_4]^+[QH]^-$	2.70

Four electronic absorptions are observed for $[Q]^{2-}$; the three higher energy absorptions are probably one transition with vibrational spacings of 2150 and 1350 cm^{-1}. The lowest energy absorption, i.e., ~16 000 cm^{-1}, is assigned to the symmetry allowed (DZ + $D_{c,o}$ basis set) HOMO → LUMO transition. This is at substantially lower energy than the comparable absorption for $[DDQ]^{2-}$, i.e., 21 000 cm^{-1}.[24] For QH_2 the HOMO → LUMO transition is also symmetry allowed (DZ + $D_{c,o}$ basis set) and is shifted to higher energy, i.e., 25 500 cm^{-1}, as observed for **Q**. The next transitions are due to the HOMO → NLUMO and the NHOMO → LUMO which should be close in energy. On the lower energy peak there is one resolved vibrational transition of 1125 cm^{-1}. For $[QH]^-$ the transitions are all allowed with the first transition at 20 000 cm^{-1} corresponding to the HOMO → LUMO transition. The next transition probably corresponds to the NHOMO → LUMO transition with the HOMO → NLUMO close in energy.

Table VI. Calculated Bond Distances, Å, for $[Q]^n$ (n = 0, 1–, 2–)

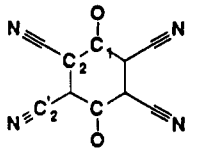

	n = 0			n = 1–			n = 2–		
	STO-3G	DZ + $D_{c,o}$	expt	STO-3G	DZ + $D_{c,o}$	expt[a]	STO-3G	DZ + $D_{c,o}$	expt[b]
C_1–C_2	1.521	1.503	1.488	1.474	1.461	1.463	1.460	1.434	1.426
C_2–C_2	1.335	1.334	1.338	1.367	1.368	1.378	1.407	1.409	1.414
C_2–$C_{2'}$	1.459	1.437	1.437	1.459	1.439	1.417	1.450	1.439	1.381
C_2≡N	1.158	1.150	1.132	1.157	1.153	1.137	1.160	1.159	1.170
C_1–O	1.223	1.184	1.204	1.253	1.216	1.233	1.266	1.252	1.268

[a] Average of $\{[Fe(C_5Me_5)_2]^{\bullet+}\}_2[Q]_2^{2-}$ and $\{[Et_4N]^+\}_2[Q]_2^{2-}$. [b] $\{[(Ph_3P)_2N]^+\}_2[Q]^{2-}$.

Table VII. Calculated Bond Distances, Å, for QH_2

distance	STO-3G	DZ + $D_{c,o}$	experimental
O–C1	1.383	1.333	1.322
C1–C2	1.403	1.393	1.413
C1–C3	1.404	1.395	1.413
C2–C3	1.400	1.397	1.372
C2–C4	1.457	1.438	1.524
C3–C5	1.459	1.439	1.524
O–H	0.989	0.950	0.91
C4–N	1.157	1.151	0.848
C5–N	1.158	1.152	0.848

Table VIII. Calculated Bond Distances, Å, for $[QH]^-$

distance	STO-3G	DZ + $D_{c,o}$ (C_s)	DZ + $D_{c,o}$ (C_1)	$[n\text{-}Bu_4N]^+$
O3–C1	1.409	1.361	1.361	1.350
C1–C5	1.405	1.397	1.397	1.405
C1–C7	1.398	1.386	1.386	1.405
C5–C6	1.382	1.388	1.388	1.398
C7–C8	1.390	1.400	1.400	1.398
O4–C2	1.240	1.224	1.225	1.253
C2–C6	1.486	1.454	1.455	1.438
C2–C8	1.480	1.443	1.443	1.438
O3–H1	0.989	0.947	0.948	
C5–C9	1.438	1.444	1.445	1.438
C6–C10	1.449	1.436	1.436	1.438
C7–C11	1.468	1.444	1.444	1.438
C8–C12	1.446	1.433	1.433	1.438
C9–N	1.151	1.153	1.153	1.145
C10–N	1.152	1.155	1.155	1.145
C11–N	1.152	1.154	1.154	1.145
C12–N	1.151	1.156	1.156	1.145

Although the electronic spectrum of QH_2 is qualitatively similar to that of **Q**, these spectra are indeed different. The lowest energy absorption for QH_2 corresponds to an allowed HOMO → LUMO transition and occurs at a slightly lower energy than the NHOMO → LUMO transition of **Q** as expected from the orbital energy differences (vide supra). The next-lowest energy transition corresponds to either the NHOMO → LUMO or HOMO → NLUMO, both of which are allowed. The resolved vibrational transition of 1125 cm^{-1} in the band at 36 900 cm^{-1} of QH_2 is clearly smaller than the 1270 cm^{-1} value observed for **Q**.

Magnetic Properties. Magnetic Susceptibility. QH_2 and **Q** as well as the compounds containing $[QH]^-$ and $[Q]^{2-}$ are diamagnetic with susceptibilities consistent with that calculated from Pascal constants (i.e., -104×10^{-6} emu/mol for **Q**). Salts formally containing $[Q]^{\bullet-}$ with diamagnetic cations are also diamagnetic and suggest that $[Q]^{\bullet-}$ dimerized as $[Q]_2^{2-}$ as found for the $[Et_4N]^+$ and $[Fe(C_5Me_5)_2]^{\bullet+}$ salts. Likewise, [TTF][Q] was diamagnetic, and this was attributed to dimerization of both the cation and the anion. Such $[TTF]_2^{2+}$ dimers have been previously structurally characterized.[31]

Table IX. Charge Distributions for $[Q]^n$ (n = 0, 1–, 2–), $[QH]^-$, and QH_2

	n = 0		n = 1–		n = 2–	
atom	STO-3G	DZ + $D_{c,o}$	STO-3G	DZ + $D_{c,o}$	STO-3G	DZ + $D_{c,o}$
			$[Q]^n$ (n = 0, 1–, 2–)			
C1	0.21	0.24	0.14	0.22	0.12	0.18
O	–0.15	–0.25	–0.29	–0.41	–0.45	–0.58
C2	0.03	0.07	–0.02	0.00	–0.08	–0.06
C2′	0.08	–0.08	0.07	–0.06	0.06	–0.04
N	–0.14	0.01	–0.23	–0.10	–0.32	0.21

atom	STO-3G	DZ + $D_{c,o}$ (C_s)	DZ + $D_{c,o}$ (C_1)
		$[QH]^-$	
O3	–0.29	–0.60	–0.60
O4	–0.35	–0.48	–0.48
H1	0.19	0.48	0.48
C1	0.06	0.12	0.12
C2	0.18	0.21	0.22
C5	0.01	0.10	0.11
C6	–0.06	–0.05	–0.05
C7	0.00	0.11	0.11
C8	–0.07	–0.10	–0.10
C9	0.08	–0.08	–0.08
C10	0.07	–0.06	–0.06
C11	0.06	–0.16	–0.16
C12	0.06	–0.05	–0.05
N-9	–0.22	–0.13	–0.13
N-10	–0.25	–0.09	–0.09
N-11	–0.22	–0.10	–0.10
N-12	–0.25	–0.12	–0.12

atom	STO-3G	DZ + $D_{c,o}$
	QH_2	
O	–0.25	–0.56
C1	0.16	0.17
C2	0.02	0.07
C3	0.01	0.11
C4	0.08	–0.09
C5	0.06	–0.19
H	0.23	0.50
N-4	–0.15	0.00
N-5	–0.15	–0.02

The 2–320 K Faraday balance susceptibility[13] of $[Fe(C_5H_5)_2][Q]$, $[Fe(C_5Me_5)_2][H]^+[Q]^{2-}$, $[Fe(C_5Me)_2][Q]$, and $[Fe(C_5HMe_4)_2][QH]$ can be fit by the Curie–Weiss law, $\chi_M = C/(T - \theta)$ with effective moments, μ_{eff} of 2.74, 3.06, 2.64, and 2.99 μ_B and θ of –2.2, –0.6, –4.1, and –0.5 K, respectively. The value of μ_{eff} indicates that there is only one $S = {}^1/_2$ radical per formula unit contributing to the susceptibility. This is consistent with the structures possessing $S = 0$ $[Q]_2^{2-}$, i.e., only the radical cations

(31) Mayerle, J. J.; Torrance, J. B. *Bull. Chem. Soc. Jpn.* **1981**, *54*, 3170.

Table X. Experimental (Nujol) and Calculated ν(C≡N) Stretching Frequencies, cm⁻¹

compound	ν_{obs}[a]	ν_{calc}	ν_{scaled}	I_{calc}, km/mol	sym
Q	2241 w (CH_2Cl_2)	2550	2244	0.3	b_{3u}
	2210 w (CH_2Cl_2)	2544	2239	2.2	b_{2u}
	2244 s R	2549	2243	0.0	b_{1g}
		2545	2240	0.0	a_g
$[\mathbf{Q}]^{\bullet-}$	2216 m[b] (MeCN)	2510	2209	92	b_{3u}
		2504	2204	530	b_{2u}
		2514	2212	0.0	b_{1g}
		2513	2211	0.0	a_g
$[\mathbf{Q}]_2^{2-}$	2217 m[c] and 2226 sh[c]				
$[\mathbf{Q}]^{2-}$	2185 s[d]	2446	2152	205	b_{3u}
	2195 w[d]	2442	2149	1515	b_{2u}
	2197 s R[h]	2459	2164	0.0	a_g
		2455	2160	0.0	b_{1g}
$[H]^+[\mathbf{Q}]^{2-}$	2230 w,[e] 2224 sh,[f] 2240 s[g]	2446	2152	205	b_{3u}
	2216 m,[e] 2219 m[f]	2442	2149	1515	b_{2u}
	2237 s R,[g] 2247 m R[g]	2459	2164	0.0	a_g
	2202 s R,[h] 2216 s R,[h] 2229 s[h] R	2455	2169	0.0	b_{1g}
$[\mathbf{QH}]^-$	2236 w,[i] 2231 m[h]	2519	2217	53	a
	2222 m, 2220 m,[h] 2207 m[h]	2498	2198	30	a
		2494	2195	193	a
		2482	2184	236	a
$[\mathbf{QH}_2]$	2263 m, 2241 m	2539	2234	27	b_u
	2262 m, 2237 s, 2231 s R	2525	2222	44	b_u
	2230 s[j]	2538	2233	0.0	a_g
		2525	2222	0.0	a_g

[a] IR unless noted R (Raman, neat); scale factor = 0.88 (see text). [b] $\{[NEt_4]^+\}_2[\mathbf{Q}]_2\}^{2-}$ in solution. [c] Average of $\{[NEt_4]^+\}_2[\mathbf{Q}]_2\}^{2-}$ and $\{[Fe(C_5Me_5)_2]^{\bullet+}\}_2[\mathbf{Q}]_2\}^{2-}$ salts. [d] Average for the $[n\text{-}Bu_4N]^+$, $[NEt_4]^+$, $[Co(C_5Me_5)_2]^+$, and $[(PPh_3)_2N]^+$ salts. [e] $[Fe(C_5Me_5)_2]^{\bullet+}[H^+][\mathbf{Q}]^{2-}$. [f] $[NMe_4]^+[H]^+[\mathbf{Q}]^{2-}$. [g] $Na^+[H]^+[\mathbf{Q}]^{2-}$. [h] $[n\text{-}Bu_4N]^+[\mathbf{QH}]^-$. [i] $[NEt_4]^+[\mathbf{QH}]^-$. [j] $Ag_2\mathbf{Q}$. [k] $\{[NEt_4]^+\}_2[\mathbf{Q}]_2\}^{2-}$.

Table XI. Electronic Absorption Spectral Parameters for Q, QH_2, $[QH]^-$, $[Q]^{\bullet-}$, and $[Q]^{2-}$

absorption maxima, λ_{max}, nm	absorption maxima, λ_{max}, cm^{-1}	molar extinction, ϵ, $cm^{-1}\ M^{-1}$
	Q[a]	
372	26 880	2 640
271	36 900	4 155
262	38 170	4 220
237	42 195	7 140
	$\mathbf{QH}_2$[b]	
392	25 500	10 500
271	36 900	11 250
263	38 025	10 100
240	41 670	23 775
215	46 500	45 800
	$[\mathbf{Q}]^{\bullet-}$ [b,c]	
750	13 300	9 000
660 sh	15 150	3 650
486	20 575	5 240
452	22 125	4 600
424 sh	23 585	2 170
363	27 550	7 670
338 sh	29 585	2 380
292	34 250	1 450
276	36 230	6 880
258	38 760	19 260
254	39 370	19 200
	$[\mathbf{QH}]^-$ [b,c]	
500	20 000	13 175
273	36 630	18 575
248	40 325	10 750
211	47 400	26 600
	$[\mathbf{Q}]^{2-}$ [b,d]	
640	15 625	20 300
309	32 350	8 560
290	34 500	16 800
279	35 850	18 750

[a] CH_2Cl_2. [b] MeCN. [c] As the $[Et_4N]^+$ salt. [d] Average for the $[n\text{-}Bu_4N]^+$ and $[NEt_4]^+$ salts.

contribute to the magnetic susceptibility. The linearity of the χ^{-1} vs T plots argues that the singlet–triplet energy gap for $[\mathbf{Q}]_2^{2-}$ must be a sufficiently large (>4 kcal/mol) and that there is no detectable triplet concentration at temperatures up to 320 K.[32] The effective moments are greater than the $S = {}^1/_2$ spin-only value of 1.73 μ_B consistent with values found for ferrocenium salts of diamagnetic anions.[8b,9,33] Thus, $[\mathbf{Q}]_2^{2-}$ acts as a diamagnetic spacer between the radical cations and prevents the onset of cooperative magnetic ordering at low temperatures.

$[Cr(C_5Me_5)_2][\mathbf{QH}]$ and $[HOC][\mathbf{Q}]$ have moments of 3.73 and 1.75 μ_B, respectively. Both are consistent with only the cation contributing to the susceptibility. The former is 0.15 μ_B lower than the expectation for the $g = 2$, $S = {}^3/_2$ cation, whereas the latter is 0.02 μ_B greater than the expectation for the $g = 2$, $S = {}^1/_2$ cation.[13] The θ of +5.2 and −4.3 K respectively suggest weak ferromagnetic coupling between the cations for the former and weak antiferromagnetic coupling between the cations for the latter complex.

EPR. In solution $[\mathbf{Q}]_2^{2-}$ dissociates into $[\mathbf{Q}]^{\bullet-}$ as an intense EPR spectrum characteristic of $[\mathbf{Q}]^{\bullet-}$ is observed. The optimal resolution was obtained from $\{[Et_4N]^+\}$-$[\mathbf{Q}]_2^{2-}$(in 1:1 CH_2Cl_2/MeCN at 25 °C), Figure 21. The spectrum consists of a nonet pattern appropriate for a weak hyperfine interaction of the unpaired electron with four equivalent ^{14}N nuclei (a_{CN} = 0.32 G; g = 2.009 47). At high gain, ^{13}C satellite lines can easily be detected, Figure 21 bottom. They reveal hyperfine interactions with two of the three types of ^{13}C atoms of $[\mathbf{Q}]^{\bullet-}$ (2.58 and 5.25 G), with the third, presumably the carbonyl carbon, being too small to be observed. The results are in qualitative agreement with that reported for $[DDQ]^{\bullet-}$.[24]

The spin populations were calculated at the UHF level with the STO-3G basis set in order to obtain a qualitative analysis (Figure 22). Excess α-spin (there is one more α-

(32) A triplet EPR signal is observed for single crystals of $\{[Et_4N]^+\}_2[\mathbf{Q}]_2^{2-}$. Hynes, R. C.; Krusic, P. J.; Miller, J. S.; Preston, K. F.; Spring, J. J.; Williams, A. J., manuscript in preparation.

(33) This is due to the g value for the cation being distinctly different from two and very anisotropic; i.e., $g_\parallel \sim 4$ and $g_\perp = 1.3$.[34]

(34) Duggan, D. M.; Hendrickson, D. N. *Inorg. Chem.* **1975**, *14*, 955.

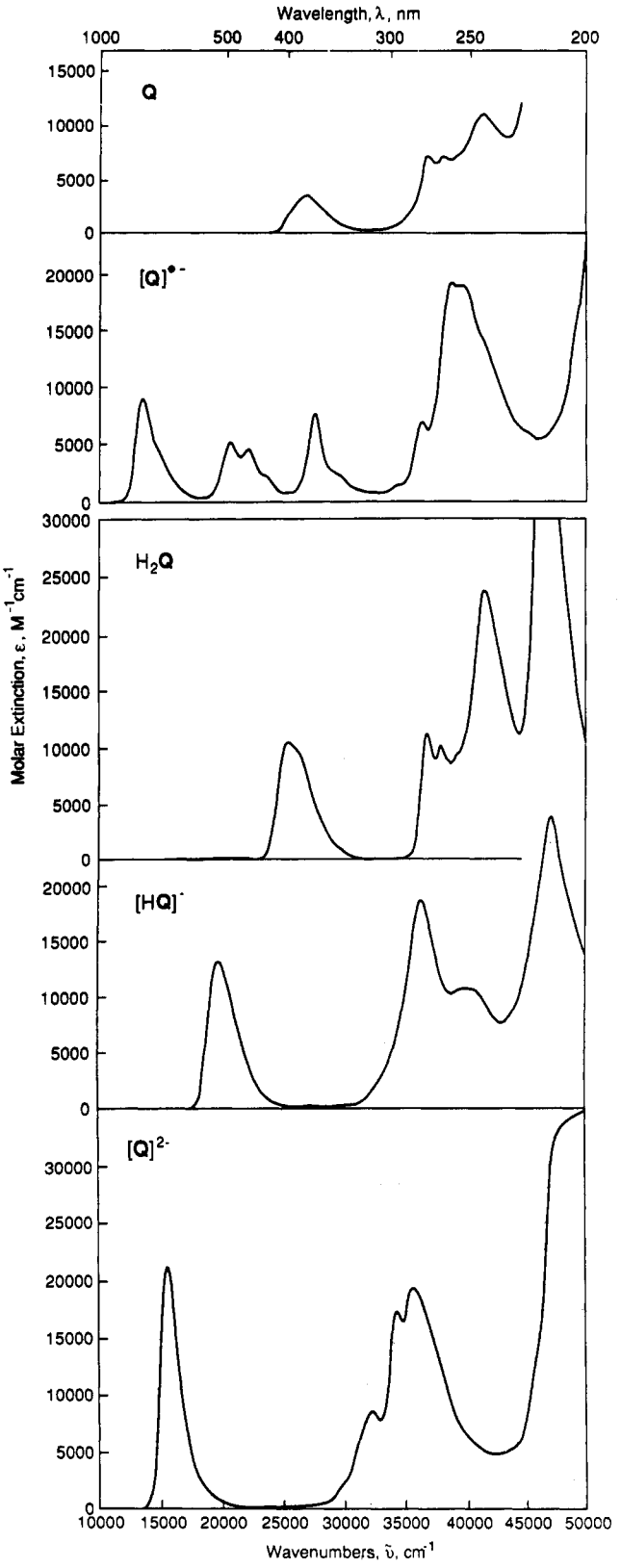

Figure 20. Electronic absorption spectra of **Q** (CH_2Cl_2), $\{[Et_4N]^+\}_2[Q]_2^{2-}$ (MeCN), $\{[Et_4N]^+\}_2[Q]^{2-}$ (MeCN), $[Et_4N]^+$-$[QH]^-$(MeCN), and QH_2 (MeCN).

than β-electron) is predicted to be found on the O, N, and the ring C's bonded to the CN groups consistent with the charge distribution. The carbons directly bonded to O or N are predicted to have excess β-spin. The EPR spectrum involves the interaction of the spin in the 2s orbitals with the nuclei. Thus, the 2s orbital spin populations are also

Table XII. Calculated Frontier Orbital[a] Energies (eV) for Q, $[Q]^{2-}$, $[QH]^-$, and QH_2

		DZ + D$_c$	STO-3G
Q	NHOMO	12.82 b_{1u}	10.24 b_{3g}
	HOMO	12.43 b_{3g}	9.79 b_{1u}
	LUMO	2.27 b_{2g}	−1.29 b_{2g}
	NLUMO	0.53 a_u	−3.33 a_u
	UMO	−2.05 b_{1u}	−6.27 b_{1u}
$[Q]^{2-}$	NHOMO	3.20 b_{3g}	−1.41 σ
	HOMO	−0.29 b_{2g}	−5.74 b_{2g}
	LUMO	−7.10 a_u	−11.98 a_u
	NLUMO	−10.36 b_{1u}	−16.44 b_{1u}
$[QH]^-$[b]	NHOMO	7.33 a″	3.98 a′
	HOMO	4.69 a″	0.70 a″
	LUMO	−3.30 a″	−7.65 a″
	NLUMO	−5.76 a″	−10.38 a″
QH_2	NHOMO	11.40 b_g	9.38 b_g
	HOMO	10.32 b_g	8.07 b_g
	LUMO	0.83 a_u	−2.62 a_u
	NLUMO	−1.25 a_u	4.57 a_u

[a] All orbitals are π-orbitals unless noted. [b] Symmetry assignments based on C_s structure. Essentially the same orbitals energies are found for the C_1 structure.

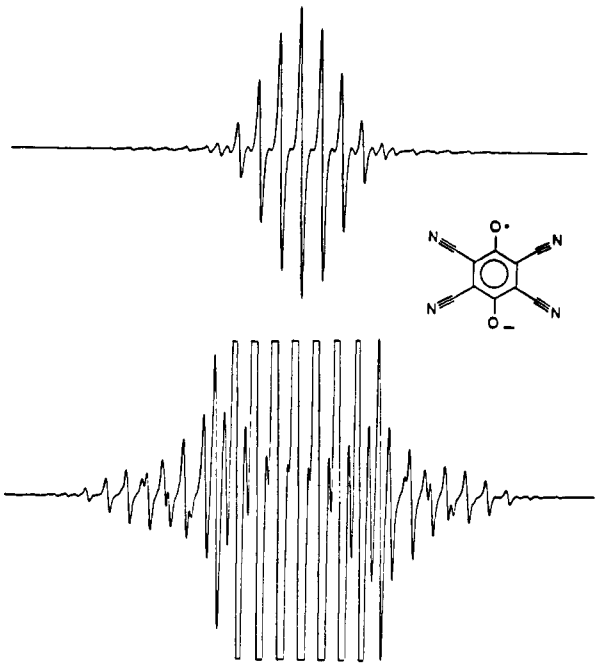

Figure 21. Solution EPR spectrum of $\{[Et_4N]^+\}_2[Q]_2^{2-}$.

presented in Figure 22. These orbital spin populations follow the same trends in terms of sign as do the total spin populations. The largest spin population in the 2s orbitals is predicted to be negative and at C1, followed by a negative 2s spin population at C2′. The O and C2 have similar positive 2s spin populations and the smallest 2s spin population is predicted for N.

Conclusion

The strong acceptor cyanil, **Q**, as well as QH_2, $[Q]^{\bullet-}$, $[QH]^-$, and $[Q]^{2-}$ have been prepared and structurally and spectroscopically characterized. **Q** is an exceptionally strong acceptor and is the strongest acceptor that has been isolated in the neutral form. It has a reduction potential 0.30 V greater than DDQ, *n*-$C_4(CN)_6$, and perfluoro-7,7,8,8-tetracyano-*p*-quinodimethane ($TCNQF_4$). Several proton-containing salts exhibit strong intermolecular hydrogen bonding with O···O separations less than 2.5 Å. The degree

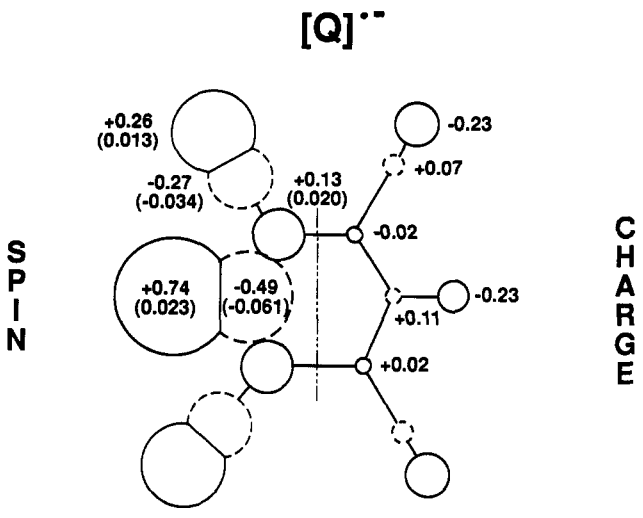

Figure 22. STO-3G basis set charge distributions and π-spin populations for $[Q]^{\bullet-}$ (2s spin densities are presented parenthetically).

of protonation varies with counterion with examples of both $[QH]^-$ and $[H]^+[Q]^{2-}$ being observed. The degree of protonation strongly influences both the electronic and $\nu(C{\equiv}N)$ IR absorptions. Electron-transfer salts readily form with many donors; however, isolation of the radical anion in the solid state has not been observed. The radical anion was structurally characterized as a diamagnetic dimer dianion, $[Q]_2^{2-}$.

Acknowledgment. We appreciate the synthetic assistance supplied by Daniel Wipf as well as the X-ray diffraction assistance by William Marshall, Faraday susceptibility data taken by R. Scott McLean, EPR by Steve Hill, F. William Barney, and Paul J. Krusic, Raman spectroscopy recorded by D. Bruce Chase, emission spectra obtained by Jonathan V. Caspar, NMR spectra taken by Fred Davidson and Derrick Ovenall, electrochemistry studies by Edward Delawski and Michael D. Ward, mass spectroscopy by Fulton Kitson, and computational assistance by Scott Walker. We are also deeply appreciative of the discussions on aspects of cyanocarbon chemistry with Owen W. Webster and hydrogen bonding with Margaret C. Etter (University of Minnesota).

Supplementary Material Available: Tables of the anion bond distances and angles, fractional coordinates/anisotropic thermal parameters, and intermolecular separations and stereoviews (103 pages). This material is contained in libraries on microfiche, immediately following this article in the microfilm version of the journal, and can be ordered from the ACS; see any current masthead page for ordering information.

Registry No. QH_2, 3533-07-1; QH_2·morpholine salt, 137415-34-0; QH_2·1,4-dioxane (1:1), 144494-17-7; $[Et_4N]^+[QH]^-$, 137415-32-8; $[Me_4N]^+[H]^+[Q]^{2-}$, 137415-33-9; QAg_2, 137443-20-0; Q, 4032-03-5; $[n\text{-}Bu_4N]^+[QH]^-$, 144494-18-8; $Na^+[H]^+[Q]^{2-}$, 144494-19-9; $[[Et_4N]^+]_2[Q]_2^{2-}$, 144494-20-2; $[Fe(C_5H_5)_2]^{\bullet+}[Q]^-$, 137415-21-5; $[Fe(C_5Me_5)_2]^{\bullet+}[H]^+[Q]^{2-}$, 144494-21-3; $[Fe(C_5HMe_4)_2]^{\bullet+}[Q]^-$, 137415-22-6; $[[Fe(C_5Me_5)_2]^{\bullet+}]_2[Q]_2^{2-}$, 137415-23-7; $[TTF]^+[Q]^-$, 137415-24-8; $[Cr(C_5Me_5)_2]^{\bullet+}[H]^+[Q]^{2-}$, 144494-22-4; $[Ru(C_5Me_5)_2]^{\bullet+}[H]^+[Q]^{2-}$, 144494-23-5; $[Co(C_5Me_5)_2]^{\bullet+}[H]^+[Q]^{2-}$, 144494-24-6; $[HOC]^+[Q]^-$, 137415-27-1; $[[Co(C_5Me_5)_2]^+]_2[Q]^{2-}$, 144494-25-7; $[[n\text{-}Bu_4N]^+]_2[Q]^{2-}$, 144494-26-8; $[[NEt_4]^+]_2[Q]^{2-}$, 144494-27-9; $[[(PPh_3)_2N]^+]_2[Q]^{2-}$ salt entry, 144494-28-0; $[[PPh_3)_2N]^+]_2[Q]^{2-}$ coordinate entry, 144494-29-1; *p*-bromanil, 488-48-2.